fermentation

MDPI

Article

Optimized Feeding Strategies for Biosurfactant Production from Acetate by *Alcanivorax borkumensis* SK2

Tobias Karmainski [1], Marie K. Lipa [1], Sonja Kubicki [2], Amina Bouchenafa [2], Stephan Thies [3], Karl-Erich Jaeger [2,3], Lars M. Blank [1] and Till Tiso [1,*]

[1] iAMB—Institute of Applied Microbiology, ABBt—Aachen Biology and Biotechnology, RWTH Aachen University, 52074 Aachen, Germany; tobias.karmainski@rwth-aachen.de (T.K.); marie.lipa@rwth-aachen.de (M.K.L.); lars.blank@rwth-aachen.de (L.M.B.)
[2] IMET—Institute of Molecular Enzyme Technology, Heinrich-Heine-Universität Düsseldorf, 40225 Düsseldorf, Germany; s.kubicki@fz-juelich.de (S.K.); a.bouchenafa@fz-juelich.de (A.B.); k.-e.jaeger@fz-juelich.de (K.-E.J.)
[3] Institute of Bio- and Geosciences, IBG-1: Biotechnology, Forschungszentrum Jülich, 52425 Jülich, Germany; s.thies@fz-juelich.de
* Correspondence: till.tiso@rwth-aachen.de

Abstract: Biosurfactants are much-discussed alternatives to petro- and oleochemical surfactants. *Alcanivorax borkumensis*, a marine, Gram-negative γ-proteobacterium, produces a glycine-glucolipid biosurfactant from hydrocarbons, pyruvate, and acetate as carbon sources. Sustainable acetate production from lignocellulose or syngas adds to its relevance for the bioeconomy. This study investigated nitrogen sources and carbon-to-nitrogen ratios (C/N) to optimize fed-batch fermentation for biosurfactant production using *A. borkumensis* with acetate as the carbon source. Urea enabled high biosurfactant production, which was confirmed in DO-based fed-batch fermentation. Varying C/N ratios led to increased glycine-glucolipid production and decreased biomass production, with improvement plateauing at a C/N ratio of 26.7 Cmol Nmol^{-1}. pH-stat fed-batch fermentation using glacial acetic acid as the carbon source and a pH-adjusting agent doubled the biosurfactant production. Finally, bubble-free membrane aeration was used to prevent extensive foam formation observed during conventional bubble aeration. The efficient production made it possible to investigate the bioactivity of glycine-glucolipid in combination with antibiotics against various microorganisms. Our findings allow for the leverage of glycine-glucolipid biosurfactant production using acetate as a carbon source.

Keywords: glycolipid; bioactivity; membrane aeration; pH-stat; fed-batch; foam formation; antifoaming agent; carbon-to-nitrogen ratio; DO-based fed-batch; bubble-free; urea

Citation: Karmainski, T.; Lipa, M.K.; Kubicki, S.; Bouchenafa, A.; Thies, S.; Jaeger, K.-E.; Blank, L.M.; Tiso, T. Optimized Feeding Strategies for Biosurfactant Production from Acetate by *Alcanivorax borkumensis* SK2. *Fermentation* **2024**, *10*, 257. https://doi.org/10.3390/fermentation10050257

Academic Editor: Nhuan Nghiem

Received: 25 March 2024
Revised: 8 May 2024
Accepted: 14 May 2024
Published: 14 May 2024

1. Introduction

Biosurfactants are amphiphilic molecules produced by various microorganisms [1,2]. This group of molecules has diverse chemical structures, represented by fatty acids, glycolipids, lipopeptides, lipoproteins, phospholipids, and polymeric biosurfactants [3]. The diverse compositions of these structures yield a range of biological and physicochemical attributes, including the effective reduction in surface tension, low critical micelle concentrations, the chelation of metal ions, bioactivity, and remarkable stability [2,4]. Biosurfactants play a vital role in enabling microorganisms to utilize hydrophobic substrates but also can contribute to the virulence of pathogens like *Pseudomonas aeruginosa* [5,6]. Biosurfactants can be derived from renewable resources, generally have low toxicity [7], and are biodegradable [8,9].

For example, the interactions of biosurfactants with antibiotics open new avenues in medical research and therapy, potentially enhancing the efficacy of existing antibiotic

treatments and reducing antibiotic use [10]. These combinatorial effects, arising from biosurfactants' unique structure and diverse biochemical properties, offer exciting prospects for innovative approaches in combating antibiotic-resistant pathogens [11]. A notable example is the synergy observed between biosurfactants and conventional antibiotics against *Staphylococcus aureus*, where the combined treatment significantly improved antibiotic efficacy, suggesting a promising strategy to overcome drug resistance [12,13].

Alcanivorax borkumensis SK2 is characterized as an aerobic, non-pathogenic, rod-shaped, Gram-negative, halophilic, γ-proteobacterium renowned for synthesizing a glycine-glucolipid biosurfactant. The strain belonging to the obligate hydrocarbonoclastic bacteria was first isolated in 1992 from seawater near the Island of Borkum and is considered highly specialized, with a relatively small genome size of 3.12 Mb [14,15]. *A. borkumensis*, being halophilic, possesses sodium-dependent transport systems that leverage the sodium gradient to facilitate nutrient uptake as an energy source [14]. It requires an optimal NaCl concentration of 3 to 10% (*w*/*v*) for growth and magnesium ions to prevent cell lysis [15]. *A. borkumensis* is known for its ability to degrade linear and branched aliphatic hydrocarbons [15–17]. While *A. borkumensis* can degrade a wide range of hydrocarbons (C_5–C_{32}), its hydrophilic substrate range is limited to acetate, propionate, and pyruvate due to the absence of key enzymes and transporters responsible for sugar utilization [14,15,18]. It can use NH_4^+ or NO_3^- as nitrogen sources, with NO_3^- converted to NH_4^+ under ATP consumption [14]. *A. borkumensis* produces various storage compounds using *n*-alkanes and hydrophilic substrates as carbon sources at a high carbon-to-nitrogen (C/N) ratio [19,20]. Genes coding for enzymes in the synthesis of storage compounds such as polyhydroxyalkanoates (PHA), wax esters (WE), and triacylglycerols (TAG) were identified in *A. borkumensis*, with a predominant production of WE and TAG [14,21,22].

The glycine-glucolipid found in *A. borkumensis* SK2 consists of four 3-hydroxy-fatty acids of different chain lengths, interconnected by ester bonds and a glycosidic linkage to the C_1-atom of glucose. Glycine forms an amide bond with the terminal 3-hydroxy-fatty acid (Figure 1) [23,24]. Earlier research indicated the existence of an extracellular glucolipid lacking glycine alongside a glycine-containing form associated with the membrane. However, recent studies have refuted the existence of the extracellular glycine-free variant [24,25]. The membrane-associated glycine-glucolipid enhances the cell surface hydrophobicity, increasing the adherence to oil/water interfaces and improving the bioavailability of hydrophobic carbon sources [26–28]. The entire biosynthesis pathway for the glycine-glucolipid in *A. borkumensis* SK2 remains to be fully understood.

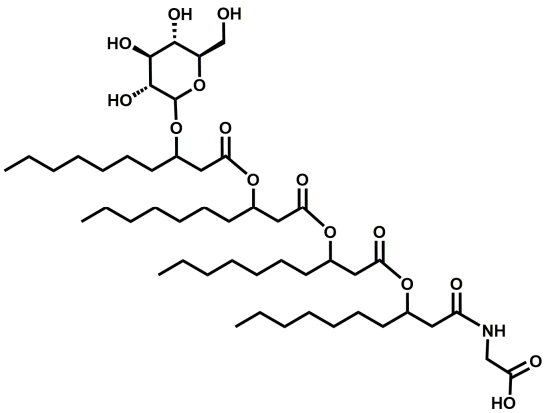

Figure 1. The structure of the glycine-glucolipid from *A. borkumensis* SK2. It contains four 3-hydroxy fatty acids interlinked by ester bonds. The hydroxy group of the first fatty acid forms a glycosidic linkage to glucose, and the terminal carboxy group is linked to glycine through an amide bond.

Only a few approaches are described to produce the *A. borkumensis* biosurfactant. A glucolipid composed of four 3-hydroxy-fatty acids and one glucose molecule without glycine was produced by nitrogen-limited fed-batch fermentation using *n*-alkanes

as substrates, resulting in a glucolipid titer of 1.7 g L^{-1} [16]. However, recent studies demonstrated that a glycine-free glucolipid apparently does not exist [24,25].

Secondary metabolites are often produced under nutrient-limiting or starving conditions, with the nitrogen source and the C/N ratio playing important roles in biosurfactant production [29]. Studies with *P. aeruginosa* show that switching to $NaNO_3$, urea or NH_4NO_3 improves rhamnolipid production compared to NH_4Cl but also results in lower biomass production due to the more cumbersome metabolism [30,31]. Regarding the C/N ratio, *P. aeruginosa* exhibits an increased rhamnolipid titer with higher C/N ratios. However, the limit of this enhancement is observed at a C/N ratio of 62 Cmol $Nmol^{-1}$ with $NaNO_3$ as the nitrogen source and glycerol as the carbon source. In general, the optimal C/N ratio is found to depend on the carbon source [32]. High C/N ratios may also trigger the production of storage molecules like TAG and WE, diverting carbon away from glycolipid production [20]. Therefore, the nitrogen source and the C/N ratio are important in biosurfactant production.

Numerous biotechnological products aim to replace petrochemicals and reduce the CO_2 footprint, relying on glucose as a carbon source [33]. However, using glucose competes with human food resources, necessitating renewable alternatives like lignocellulose or C_1-substrates [34,35]. Various reaction routes can be used to produce acetate from alternative carbon sources, including second-generation feedstocks like lignocellulose [36,37]. It can also be produced via syngas fermentation, microbial electrosynthesis, or methane oxidation [38–40]. The resulting acetate can be upcycled into higher-value products through chemical or biological processes [35,37]. The acetate uptake by organisms is either transporter-mediated by facilitated diffusion or actively through transporters under energy consumption [35,41]. Once taken up, acetate is activated to form acetyl-CoA, serving as a precursor for various metabolic pathways, including de novo fatty acid synthesis, essential for glycolipid synthesis [35,42].

Both acetic acid and acetate salts exhibit water miscibility, facilitating effortless mass transfer into the culture broth and minimizing bioreactor volume dilution when employing highly concentrated solutions or pure acetic acid for feeding. Additionally, the microbial consumption of acetate from the culture medium leads to a rise in the pH. Consequently, the pH serves as a direct online process parameter, allowing the coupling of acetate feeding in a pH-stat fed-batch fermentation with pH control using pure acetic acid as a pH agent [43,44]. However, it can also inhibit bacterial growth due to cytosol acidification and osmotic pressure effects [45,46]. Strategies to overcome acetate inhibition include modifying the growth medium, using carbon-limited fed-batch processes, dialysis, or metabolic engineering [47–50]. The biotechnological production of itaconate and rhamnolipids with acetate as the sole carbon source has been shown for several organisms like *Pseudomonas putida*, *Escherichia coli*, and *Corynebacterium glutamicum*, which were able to grow on acetate concentrations of at least 5 g L^{-1} [51–53]. Various other organisms, including *A. borkumensis*, can metabolize acetate, making it a valuable resource for sustainable biosurfactant production [15].

The production of biosurfactants by fermentation faces challenges, with foam formation being the major issue [54]. Foaming can negatively impact the overall process performance, product quality, and quantity and may lead to the loss of biocatalysts already at low product concentrations [55–57]. It also harbors risks such as blocking sterile filters, which cause overpressure and endanger sterility [58–60]. Researchers got creative to mitigate foam formation in fermentation processes, such as using antifoaming agents [61], bubble-free membrane aeration [62,63], defoamers as substrates [64,65], foam fractionation [66,67], headspace aeration in combination with overpressure [68], in situ liquid–liquid extraction [69], and mechanical foam breakers [70]. Among all the strategies mentioned, bubble-free membrane aeration changes the process minimally, as it can be carried out in the same way as with bubble aeration but without the addition of antifoaming agents or solvents for in situ extraction.

This study presents enhanced glycolipid production using *A. borkumensis* through fed-batch fermentation with acetate as the carbon source. The primary objective was to increase the glycolipid titer, specific product yields, and space-time yields. The influence of the nitrogen source and the C/N ratio was investigated to achieve this. Furthermore, a pH-stat fed-batch using glacial acetic acid was established, allowing for a highly concentrated feed without diluting the product concentration. In addition, in situ membrane aeration was used to prevent foam formation. This process strategy provided sufficient glycolipid material to test the bioactivity of the glycine-glucolipid against different microorganisms [10].

2. Materials and Methods

Initially, a DO-based fed-batch fermentation with NH_4Cl as the nitrogen source served as a benchmark. Shake flask experiments followed to study the effects of altering the nitrogen source, with insights applied to subsequent fermentations. Feeding strategy optimization included a pH-stat fed-batch using glacial acetic acid as a pH agent and carbon source and a two-stage DO-based feeding strategy. A comparative analysis of conventional bubble aeration and bubble-free membrane aeration assessed foam formation during biosurfactant production.

2.1. Bacterial Strain and Medium

The bacterial strain *Alcanivorax borkumensis* SK2 (DSM 11573) was used for all cultivation experiments [15]. Modified (mod.) ONR7a medium was used for all cultivation experiments and contained (per L) 22.79 g NaCl, 11.18 g $MgCl_2 \times 6\ H_2O$, 3.98 g Na_2SO_4, 1.46 g $CaCl_2 \times 2\ H_2O$, 11.92 g HEPES, 0.72 g KCl, 0.46 g $NaH_2PO_4 \times 2$ H2O, 83 mg NaBr, 31 mg $NaHCO_3$, 27 mg H_3BO_3, 24 mg $SrCl_2 \times 6\ H_2O$, 2.6 mg NaF, and 2 mL trace elements (500×). Trace elements contained (per L) 5.00 g $FeSO_4 \times 7\ H_2O$, 2.50 g $MnSO_4 \times H_2O$, 3.20 g $ZnCl_2$, 0.20 g $CoCl_2 \times 6\ H_2O$, 0.36 g $CuSO_4 \times 5\ H_2O$, 0.10 g $Na_2MoO_4 \times 2\ H_2O$, and 6.37 g Na_2EDTA $\times$ 2 H_2O [18,25]. Different nitrogen sources with equal amounts of nitrogen were used and are mentioned in the corresponding sections. Marine broth (Carl Roth GmbH, Karlsruhe, Germany) was autoclaved with 2% agar for plates, and sterile-filtered pyruvate at a concentration of 10 g L^{-1} was added afterward.

2.2. Cultivation Conditions

2.2.1. Pre-Culture

To initiate plate cultures, *A. borkumensis* SK2 was streaked from a cryogenic stock onto marine broth agar plates and then incubated at 30 °C for 48 to 72 h. Subsequently, the *A. borkumensis* SK2 was cultured for 20–24 h in shake flasks containing 10 mL of mod. ONR7a medium for precultures supplemented with 10 g L^{-1} pyruvate and incubated at 30 °C and 300 rpm (50 mm throw) with a 10% filling volume. Afterward, the strain was cultivated in a second shake flask in 50 mL mod. ONR7a at 300 rpm (50 mm throw) and 30 °C with 10 g L^{-1} acetate for main cultures up to an optical density (OD_{600}) of 4.0.

2.2.2. Transfer Rate Online Measurement Cultivation

This study investigated different nitrogen sources and C/N ratios using the transfer rate online measurement (TOM) shaker (Adolf Kühner AG, Birsfelden, Switzerland) for the determination of the oxygen transfer rate (OTR) in shake flasks. For TOM cultivation, 500 mL shake flasks were inoculated with 25 mL of mod. ONR7a medium containing 10 g L^{-1} acetate to an OD_{600} of 0.2 and cultivated at 30 °C and 300 rpm (50 mm throw) in duplicates. The exact conditions of each experiment can be found in Table 1.

Table 1. Specific cultivation conditions for the TOM shaker experiments. The four different nitrogen sources (urea, NH_4Cl, NH_4NO_3, and $NaNO_3$) were tested individually as the sole nitrogen source.

Carbon and Nitrogen Concentrations	Evaluation of Nitrogen Sources	Evaluation of C/N Ratios
Acetate concentration [g L^{-1}]	10	10
Nitrogen sources	Urea, NH_4Cl, NH_4NO_3, $NaNO_3$	Urea
C/N ratio [Cmol $Nmol^{-1}$]	8.9	8.9, 17.8, 26.7, 35.6, 53.4
Nitrogen source concentration [g L^{-1}]	1.1 (Urea), 2.0 (NH_4Cl), 1.5 (NH_4NO_3), 3.2 ($NaNO_3$)	1.1, 0.56, 0.37, 0.28, 0.19

2.2.3. Offline Shake Flask Cultivation

Different C/N ratios were investigated in shake flask cultivations at a lower initial acetate concentration. Then, 500 mL shake flasks were inoculated with 50 mL mod. ONR7a medium and 5 g L^{-1} acetate as a carbon source to an OD_{600} of 0.2 and cultivated at 30 °C and 300 rpm (50 mm throw) in duplicates. Different C/N ratios were investigated with urea (8.9, 17.8, 26.7, 35.6, and 53.4 Cmol $Nmol^{-1}$), which corresponded to the following urea concentrations: 0.56, 0.28, 0.19, 0.14, and 0.09 g L^{-1}.

2.3. Stirred-Tank Bioreactor Conditions

All fermentations were conducted using a 3 L BioFlo120 stirred-tank bioreactor under the control of DASware control software version 5.3.1 (both from Eppendorf AG, Hamburg, Germany). The bioreactor was fitted for online data acquisition, featuring a dissolved oxygen (DO) probe (VisiFerm DO ECS 225, Hamilton, Bonaduz, Switzerland), a pH probe (EasyFerm Plus PHI K8 225, Hamilton, Bonaduz, Switzerland), and a Pt100 temperature sensor. Foam control was achieved through a foam sensor and the addition of an antifoaming agent (Antifoam 204, Sigma Aldrich, St. Louis, MO, USA). pH was kept at 7.3 by the addition of 4 M H_2SO_4. DO levels were kept above 30% by adjusting the stirring rate automatically from 300 to 1200 min^{-1}. Airflow remained constant at 24 L h^{-1}. Exhaust gas underwent drying with an exhaust gas condenser, with O_2 and CO_2 concentrations monitored using a BlueVary Sensor and BlueVis software v4.65 (BlueSens gas sensor GmbH, Herten, Germany). The agitation shaft featured two six-blade Rushton turbines (⌀ 53 mm). A filling volume of 1.2 L was used. The batch phase was performed with mod. ONR7a medium with 5 g L^{-1} acetate and heated to 30 °C before inoculation. The bioreactor was inoculated from a pre-culture to an OD_{600} of 0.2. For the increase in the bioreactor cultivation volume, only the addition of the feeding solution was considered since H_2SO_4 addition and sampling are counterbalanced and, therefore, negligible.

Different feed solutions were used for the fed-batch processes depending on the required C/N ratio (Table 2).

Table 2. Feed solutions with varying C/N ratios for fed-batch cultivations. The benchmark condition was C/N of 8.9 Cmol $Nmol^{-1}$, and NH_4Cl and urea were used as nitrogen sources.

Feed Components	Concentration [g L^{-1}]			
	C/N of 8.9	C/N of 17.8	C/N of 26.7	Glacial Acetic Acid of C/N 17.8
Acetate	200.0	200.0	200.0	1050.0
Urea	22.4 (40 for NH_4Cl)	11.2	7.5	59.0
$NaH_2PO_4 \times 2\ H_2O$	9.2	9.2	9.2	24.2

2.3.1. Bubble-Free Stirred-Tank Bioreactor with In Situ Static Membrane Module

The conditions and parameters for temperature, pH, and inoculation in fermentations with membrane aeration were equal to those of conventional fermentations, as detailed

in Section 2.3. A poly-4-methyl-1-pentene (PMP) hollow fiber membrane (Oxyplus, 3M, Neuss, Germany) was selected as the membrane material. The BT Membrane Module Static 2L (BioThrust GmbH, Aachen, Germany) was utilized [62], containing approximately 1430 membrane fibers with a combined length of 163 m and a total membrane area of 0.195 m^2. No foam sensor or antifoaming agent was employed in this setup. The agitation shaft was outfitted with three Rushton turbines and a pitched blade turbine, while the filling volume was raised to 2 L. Before utilization, the membrane module underwent sterilization with 70% ethanol and was subsequently placed in the autoclaved bioreactor under sterile conditions. A steady gas flow of 60 L h^{-1} and an unchanging agitation speed of 300 min^{-1} were sustained. To ensure a DO setpoint of 30%, the transmembrane pressure (TMP) was incrementally increased from 0 to 0.3 bar, and an automatic DO cascade control was implemented with X_{O2} ranging from 21 to 100% oxygen.

2.3.2. DO-Based Fed-Batch Fermentation

DO-based fed-batch fermentation was started in batch mode and switched to fed-batch mode after acetate depletion, indicated by an increase in the DO from 30% to over 70%. This fed-batch strategy was performed with both the bubble-aerated and the membrane-aerated reactor setup. The only difference was that the membrane reactor had a higher filling volume. Hence, the feeding rates had to be relatively adapted to the higher volume, resulting in higher feeding rates. The feed rate was 26 mL h^{-1} (43 mL h^{-1} for the membrane process) at a DO above 70% and stopped below 40%. If the DO decreased below 15%, the agitation rate was automatically increased by 50 min^{-1}. If the biomass and the off-gas CO_2 concentration curves flattened, the feed rate was increased by 13 mL h^{-1} (26 mL h^{-1} for the membrane process) and then by 6.5 mL h^{-1} (13 mL h^{-1} for the membrane process). A total of 50 g acetate was fed. In addition, 2.4 mL (4 mL for the membrane process) of a 500× trace element solution was manually pulsed at an OD_{600} of 8.0 and 12.0. An overview of the DO-based fed-batch fermentations with different feeding strategies can be found in Table 3. In Table 3, conditions from benchmark fermentations conducted in the batch phase using 2.0 g L^{-1} NH_4Cl or 1.2 g L^{-1} urea as the nitrogen source are shown. Subsequently, a fed-batch phase was initiated, where an acetate feed containing 50 g of acetate in a C/N ratio of 8.9 Cmol $Nmol^{-1}$ with NH_4Cl and urea (Table 2) was compared.

Table 3. Overview of the different fed-batch fermentations. $C_{N,batch}$ = nitrogen source concentration during the batch phase.

Fed-Batch Fermentations	$C_{N,batch}$ [g L^{-1}]	Feeding Strategy	Total Acetate Fed [g]	pH Agent
Benchmark NH_4Cl with C/N of 8.9	2.0 NH_4Cl	Feed with C/N of 8.9	50	4 M H_2SO_4
Benchmark urea with C/N of 8.9	1.12 urea	Feed with C/N of 8.9	50	4 M H_2SO_4
Urea with C/N of 17.8	0.75 urea	Feed with C/N of 17.8	50	4 M H_2SO_4
Urea two-stage feed strategy with C/N of 17.8	0.75 urea	Feed with C/N of 8.9 Feed with C/N of 17.8	25 25	4 M H_2SO_4
Urea two-stage feed strategy with C/N of 26.7	0.75 urea	Feed with C/N of 8.9 Feed with C/N of 26.7	25 25	4 M H_2SO_4
Glacial acetic acid feed with C/N of 17.8	0.75 urea	Feed with C/N of 8.9 Glacial acetic acid feed with C/N of 17.8	56–59	4 M H_2SO_4, glacial acetic acid

To investigate the impact of nitrogen-limited conditions, the initial urea batch concentration in the batch phase was reduced to 0.75 g L^{-1} to ensure complete consumption of the nitrogen source by the end of the batch phase. Following the batch phase, a feed with a C/N ratio of 17.8 Cmol $Nmol^{-1}$ was employed. In subsequent fermentations, a two-stage feed strategy was employed. The first stage involved the addition of 25 g of acetate with a C/N ratio of 8.9 Cmol $Nmol^{-1}$ (representing the original unlimited condition) at the end

of the batch phase, followed by the addition of 25 g of acetate with a C/N ratio of 17.8 or 26.7 Cmol $Nmol^{-1}$ during the second stage. The feed rate was not increased further after starting the second feed.

2.3.3. pH-Stat Fed-Batch Fermentation with Glacial Acetic Acid

In these fermentations, the batch phase was conducted with 4 M H_2SO_4 as the pH-adjusting agent. After acetate depletion in the batch phase, glacial acetic acid, containing urea and phosphate at a C/N ratio of 17.8 Cmol $Nmol^{-1}$ (Table 2), was used as a pH agent and carbon source feed, as shown in Table 3. Once the pH rose above 7.35, glacial acetic acid was added. During the first 15 h of the fed-batch phase, an additional 1.2–2.4 g of acetate feed (6–12 mL) with a C/N ratio of 8.9 Cmol $Nmol^{-1}$ (Table 2) was pulsed each time the carbon addition from glacial acetic acid was insufficient. This was indicated by a decrease in the agitation rate or an increase in DO.

2.4. Analytics

2.4.1. Optical Density

The optical density measurement at 600 nm was carried out using an Ultrospec 10 cell density meter (Amersham Biosciences, Amersham, UK), with ultrapure water utilized as the blank reference.

2.4.2. Cell Dry Weight

To ascertain the cell dry weight (CDW), a 1 mL sample of the culture broth underwent centrifugation at 4 °C and 21,130× *g* for 5 min. The resultant supernatant was subsequently poured into another sample tube for substrate determinations. Following this, the pellet was resuspended with 1 mL of ultrapure water and centrifuged again under identical conditions, with the supernatant discarded after that. The pellet was then suspended in 1 mL of ultrapure water and poured into a pre-weighed and pre-dried HPLC vial. The HPLC vial was dried for 48 h at 65 °C. Finally, the CDW was determined by weighing the sample.

2.4.3. Ammonium Quantification

The filtered supernatant samples underwent a 1:20 dilution with ultrapure water. A calibration dilution series was prepared using NH_4Cl, ranging from 400 mg L^{-1} to 6.3 mg L^{-1}. For this procedure, 10 µL of either the calibration standards or the diluted samples was poured into a 96-well plate. Then, 200 µL of a reagent solution containing 17.98 g L^{-1} Na_3PO_4, 32 g L^{-1} sodium salicylate, and 0.5 g L^{-1} sodium nitroprusside was added. Subsequently, 50 µL of 5% NaClO was pipetted into each well, and the plate was incubated at room temperature for 10 min [71]. After the incubation period, the plate was shaken for 30 s, and the absorbance of each well was measured at 685 nm using a Synergy Mx monochromator-based multimode microplate reader controlled by Gen5 software (both from BioTek Instruments, Inc., Winooski, VT, USA).

2.4.4. Acetate Quantification via HPLC

The measurement of acetate concentrations was carried out using an Ultimate 3000 HPLC system (Thermo Scientific, Waltham, MA, USA) employing an isocratic method with 5 mM H_2SO_4 as the mobile phase and a flow rate of 0.5 mL min^{-1}. Prior to HPLC analysis, the supernatant obtained after centrifugation (21,130× *g*, 5 min) was filtered through a syringe filter (0.22 µm cellulose-acetate-membrane, EXCALIBUR, Kitchener, ON, Canada). A 5 µL volume was injected for analysis using a Metab-AAC column (Ion exchange, 300 × 7.8 mm, 10 µm particle size; Isera GmbH, Düren, Germany). The column oven was set at 40 °C, and detection was carried out using a UV detector at 210 nm.

2.4.5. Urea Quantification via HPLC

The filtered supernatant was diluted at a 1:4 ratio using a 66.7% acetonitrile–water solution to measure urea concentration. Subsequently, the mixture was incubated at 4 °C for >12 h to induce protein precipitation. After incubation, the samples were centrifuged at 17,000× *g* for 2 min and filtered through a 0.22 µm regenerated cellulose membrane syringe filter (Phenomenex, Torrance, CA, USA).

The urea concentration analysis was conducted using an Ultimate 3000 HPLC system equipped with an E150/2 Nucleodur HILIC column (hydrophilic interaction liquid chromatography; 150 × 2 mm, 3 µm particle size; Macherey-Nagel GmbH & Co. KG, Düren, Germany). The column was operated at 40 °C, and an injection volume of 3 µL was used. The separation process employed an analytical gradient with 100% acetonitrile (A) and water (B) as the mobile phase, with a flow rate of 0.3 mL min^{-1}. The measurement took 17.5 min and started with a ratio of 90% A and 10% B. Within 4 min, the ratio of A was increased to 93.2%, kept constant for 0.5 min, and then decreased to 80% within another 0.5 min. This ratio was maintained for 9 min, after which it was increased back to 90% within 0.5 min and held constant until the end of the measurement. A UV detector at 200 nm was utilized.

2.4.6. Glycolipid Extraction and Purification

For the extraction of glycine-glucolipids and aglycones [24], 800 µL of the culture broth was withdrawn, and the pH was lowered to 3.0 by adding 1 M HCl. Following this, the samples were combined with 800 µL of ethyl acetate and mixed on a vortexer for 10 min. Subsequently, the mixture underwent centrifugation at 17,000× *g* for 2 min, separating the upper organic phase, which was transferred to a 15 mL tube. This extraction process was repeated twice. The tubes containing the organic phase were then subjected to evaporation using a Scan Speed 40 speed vac (Scanspeed, Lynge, Denmark) operating at 800 min^{-1}, 20 °C, and 20 mbar for a minimum duration of 3 h.

Following this, 150 µL of chloroform was introduced into the tubes to purify the dried samples [24]. A CHROMABOND SiOH silica gel column (200 mg/3 mL, 55 µm, Macherey-Nagel GmbH & Co. KG, Düren, Germany) was pre-conditioned with eight-column bed volumes of chloroform (2.4 mL). The sample was then loaded onto the column and washed with 2.4 mL of chloroform. The glycolipids were subsequently eluted into a new 15 mL tube using 13.3 column volumes (4 mL) of acetone/isopropanol (9 + 1, *v*/*v*). The eluate-containing glycolipids and acetone/isopropanol evaporated under the same conditions as the initial extraction. Finally, the dried samples were mixed with 100 µL of acetone/isopropanol (9 + 1, *v*/*v*) using a vortexer.

2.4.7. Glycolipid Quantification via HPLC

Glycine-glucolipid and aglycone concentrations were quantified using an Ultimate 3000 HPLC System equipped with a Corona Veo Charged Aerosol Detector (Thermo Scientific, Waltham, MA, USA). The analysis utilized a Nucleodur C18 Gravity column (150 × 3 mm, 3 µm particle size; Macherey-Nagel GmbH & Co. KG, Düren, Germany) with the column oven maintained at 60 °C. A 5 µL injection volume was employed. The mobile phase consisted of a solution of 0.2% formic acid (A) and acetonitrile with 0.2% formic acid (B) at a flow rate of 0.633 mL min^{-1}.

The procedure extended over a duration of 46 min and encompassed both an analytical and an inverse gradient. In the analytical gradient, the initial composition comprised 24% A and 76% B for 0.5 min, followed by a gradual increase in B to 100% over 36 min, maintaining this ratio for 5 min. Subsequently, within 0.5 min, the ratio reverted to 24% A and 76% B, remaining constant until the method's conclusion. Conversely, the inverse gradient, facilitated by Chromeleon software (Version 7.2.10, Thermo Scientific, Waltham, MA, USA), operated in "keep solvent composition" mode, resulting in a flow rate of also 0.633 mL min^{-1}. This inverse gradient, with an offset volume of 778 µL, initiated with 100% B for 1.7 min, followed by a gradual reduction of B while simultaneously increasing

A to 24% over 36 min. The ratio of 24% A and 76% B persisted until 37.7 min, at which point it transitioned back to 100% B within 0.5 min, maintaining this composition until the end of the measurement [24].

Throughout Section 3, the term "glycolipids" refers to the natural mixture produced, which contains a small amount of aglycones in addition to the glycine-glucolipids.

2.5. Checkerboard Growth Inhibition and Survival Assay

The microdilution method was employed, which refers to the broth dilution method in microtiter plates with a minimum capacity of ≤200 µL per well. Test compounds (purified glycine-glucolipid, tetracycline, and chloramphenicol) were dissolved in DMSO, and serial dilutions (1:2) were carried out. Overnight cultures of various bacterial strains, including *Corynebacterium glutamicum* ATTC 13032 (DMS 20300), *P. aeruginosa* (DMS 1117), *Serratia marcescens* (DMS 30121), *Staphylococcus epidermidis* (DMS 1798), *Staphylococcus aureus* (DMS 1104), and *Enterococcus faecium* (DMS 2146) were inoculated in 10 mL Mueller–Hinton (MH) medium (MERCK KGaA, Darmstadt, Germany) in 100 mL shake flasks and incubated at 37 °C under agitation at 130 rpm (25 mm throw). The MH medium contained (per L) 2.0 g beef extract, 17.5 g casein hydrolysate, and 1.5 g starch. The cultures were then diluted to an OD_{750} of 0.1 in MH medium (dilution 1). Given the bacteria-specific sizes, shapes, and growth behaviors under identical conditions, additional strain-specific dilutions were performed as follows: *C. glutamicum* (1:50), *S. aureus* (1:100), *S. epidermidis* (1:100), *E. faecium* (1:100), *P. aeruginosa* (1:200), and *S. marcescens* (1:200). A density of around 1×10^6 CFU mL^{-1} was achieved. The cell suspensions were transferred to 96-well VWR Multiwell cell culture plates (VWR International, Radnor, PA, USA), 50 µL per well. Each well was additionally supplemented with 3 µL of DMSO containing the compound(s) to be tested and 47 µL of the MH medium. Plates were sealed with sterile, breathable rayon film seals (VWR International, Radnor, PA, USA) and incubated at saturated humidity for 20 h at 37 °C. Afterward, the OD_{750} was measured in a SpectraMax i3x multimode microplate reader (Molecular Devices LLC, San Jose, CA, USA) at a wavelength of 750 nm using the absorbance of the medium control as reference. To standardize the presentation of the biomass between different bacterial strains, the A_{750nm} of the DMSO-only control of the respective strain in the individual experiment was set as 100% relative biomass. The minimal inhibitory concentrations (MICs) were determined as the lowest concentration showing <5% growth, and the half-maximal inhibitory concentration (IC50) was identified at 50% relative biomass.

3. Results

Biosurfactants hold significant promise as valuable products in the bioeconomy. In this study, various optimization approaches were explored to enhance the biosurfactant productivity of *A. borkumensis* SK2. First, DO-based fed-batch fermentation with the standard nitrogen source NH_4Cl was established to have a benchmark for comparison. Then, the shake flask experiments involved testing the impact of altering and limiting the nitrogen source. These experimental findings were subsequently applied in fed-batch fermentations. Furthermore, the feed strategy was optimized by investigating a pH-stat fed-batch utilizing glacial acetic acid as a pH agent and carbon source and a two-stage feed strategy based on the DO levels. Furthermore, conventional bubble aeration and bubble-free membrane aeration via an in situ membrane module were compared in terms of foam formation during biosurfactant production.

3.1. Fed-Batch Fermentation Increases Glycolipid Titers

Recently, the batch fermentation of *A. borkumensis* SK2 using acetate as carbon source in a 3 L bioreactor yielded a glycolipid titer of 43 mg L^{-1} [18]. In order to further increase the glycolipid titer, a DO-based fed-batch based on the findings from the batch fermentation was developed here.

3.1.1. DO-Based Fed-Batch—A Working Process with Bubble Aeration

The fed-batch fermentation was started with 5 g L^{-1} acetate and 2 g L^{-1} NH_4Cl. After 26 h, once the acetate from the batch phase was depleted, DO-based feeding was initiated, supplying 0.25 L feed solution with a C/N ratio of 8.9 Cmol $Nmol^{-1}$. In the remainder of Section 3, data regarding fed-batch fermentations are presented as masses, not as concentrations, since the cultivation volume was not constant over the fermentation. The volume increase and the resulting dilution of the fermentation broth by the feed were not negligible at 21% of the initial cultivation volume. Throughout Section 3, the term "glycolipids" refers to the natural mixture produced, which contains a small amount of aglycones in addition to the glycine-glucolipids.

During the batch phase, the OTR_{max} peaked at around 14 mmol L^{-1} h^{-1}, and the CDW reached 1.5 g L^{-1} with a μ_{max} of 0.15 h^{-1} (Figure S1B,C). In contrast, the glycolipid concentration increased only slightly during the batch phase to only 2 mg L^{-1}. The acetate depletion led to a rise in DO levels above 80%, triggering the initiation of automatic feed addition in fed-batch mode (Figure S1A). The OTR and CTR increased with increasing biomass, peaking at an OTR_{max} of 38 mmol L^{-1} h^{-1}. Within the 30 h fed-batch phase, 50 g of acetate was fed. The NH_4^+ was not entirely consumed during the cultivation and increased during the fed-batch phase due to excess NH_4Cl in the feed (Figure S1C). During the fed-batch phase, the glycolipid amount increased in correlation with the rising CDW, reaching a peak of 220 mg (Table 4).

Table 4. Comparison of mean performance parameters from all fed-batch fermentations conducted in this study (n = 2). With $V_{L,end}$ = cultivation volume at the end of the fed-batch process; $c_{Glycolipids}$ = glycolipid concentration at the end of the cultivation; $m_{Glycolipids}$ = glycolipid amount at the end of the cultivation; $Y_{X/S}$ = overall biomass-to-substrate yield; $Y_{P/S}$ = overall product-to-substrate yield; $Y_{P/X}$ = overall product-to-biomass yield; STY = space-time yield.

Process	Time [h]	$V_{L,end}$ [L]	Total Acetate Fed [g]	$c_{Glycolipids}$ [mg L^{-1}]	$m_{Glycolipids}$ [mg]	$Y_{X/S}$ [g g^{-1}]	$Y_{P/S}$ [mg g^{-1}]	$Y_{P/X}$ [mg g^{-1}]	STY [mg L^{-1} h^{-1}]
NH_4Cl benchmark C/N 8.9	56	1.45	50	152	220	0.36	3.9	11.0	2.7
Membrane-aerated NH_4Cl benchmark C/N 8.9	48	2.22	50	66	146	0.24	2.6	11.1	1.4
Urea benchmark C/N 8.9	60	1.45	50	183	266	0.38	5.0	13.0	3.1
Urea one-stage feeding C/N 17.8	74	1.45	50	278	403	0.23	9.0	39.0	3.8
Urea two-stage feeding C/N 17.8	63	1.45	50	260	377	0.28	7.2	26.0	4.2
Urea two-stage feeding C/N 26.7	71	1.45	50	295	428	0.25	8.0	32.1	4.2
Urea pH-stat C/N 17.8	60	1.20	56	427	512	0.22	8.2	36.8	7.1
Membrane-aerated urea pH-stat C/N 17.8	59	2.00	54	261	521	0.27	8.1	30.5	4.4

3.1.2. Membrane Aeration Sustains Foam-Free Fermentation but with Performance Losses

The filling volume was augmented to 2 L to ensure complete coverage of the entire membrane module with liquid, and the O_2 concentration in the supply gas was automatically elevated using a DO cascade to meet the oxygen requirements of *A. borkumensis*. The DO-based fed-batch fermentation lasted 48 h and was performed with 5 g L^{-1} acetate as the starting concentration.

The trend of DO correlated with that of CO_2 in the off-gas and CDW, which increased exponentially to 1.2 g L^{-1} with a μ_{max} of 0.16 h^{-1} (Figure S2B,C). At the end of the batch phase, 1.3 mg L^{-1} glycolipids were produced by *A. borkumensis*. Acetate was depleted after 30 h. During the DO-based fed-batch phase, the DO varied from about 12% when acetate was consumed to 115% when acetate was depleted (Figure S2A). To ensure oxygen supply at DO 30% due to continuous growth, the X_{O2} was increased automatically to 100% after 46.5 h and was supported by additionally increasing the stirring rate from 300 to 375 min^{-1}. Exhaust CO_2 content and CDW increased linearly during the fed-batch phase, reaching a maximum CDW of 13 g. The biomass was 7 g lower compared to bubble aeration (Figure S2C), despite the higher fermentation volume. Also, the amount of glycolipid at the end of the fed-batch phase was 146 mg, 74 mg less than in the bubble-aerated process (Table 4). The observed difference in glycolipid production between the fermentations with and without membrane aeration can be attributed to the lower amount of acetate fed in relation to the cultivation volume. Attempts to address this issue by increasing the feed rate were unsuccessful. Furthermore, the acetate concentration in the feed could not be increased further, as the maximal solubility of 200 g L^{-1} acetate was reached.

This experiment demonstrated that the fed-batch process with the membrane module works without antifoaming agent usage and oxygen limitation. As the data from the benchmark processes showed, nitrogen was present in the medium in excess over the entire cultivation period. In the feed phase, the nitrogen concentration increases over time. This high nitrogen amount favors the formation of biomass. It is known that secondary metabolites such as biosurfactants are produced more efficiently under nitrogen-starvation or nitrogen-limiting conditions [30,72,73]. Therefore, the process has been further optimized regarding the nitrogen source.

3.2. Changing the Nitrogen Sources Leads to Improved Glycolipid Production

Shake flask experiments were conducted to assess the impact of four different nitrogen sources on glycolipid production. Subsequently, the most effective nitrogen source identified from these experiments was further validated in a DO-based fed-batch fermentation.

3.2.1. A Promising Nitrogen Source—Urea

Four different nitrogen sources, namely urea ($CO(NH_2)_2$), ammonium chloride (NH_4Cl), ammonium nitrate (NH_4NO_3), and sodium nitrate ($NaNO_3$), were compared in a TOM cultivation with 10 g L^{-1} acetate and an equimolar nitrogen concentration at a C/N ratio of 8.9 Cmol $Nmol^{-1}$.

The OTR (Figure 2A) for NH_4Cl displayed an exponential increase after a short lag phase, with a μ_{max} of 0.16 h^{-1}, leading to an OTR_{max} of 18 mmol L^{-1} h^{-1}. This was reflected in the highest CDW for all nitrogen sources, reaching 3.3 g L^{-1} and a biomass-to-substrate yield ($Y_{X/S}$) of 0.33 g g^{-1} (Figure 2B). A similar OTR course was observed for the cultivations with urea and NH_4NO_3, characterized by an additional peak during slightly faster exponential growth with μ_{max} values of 0.18 h^{-1} and 0.19 h^{-1}, respectively. These approaches also exhibited lower OTR_{max} values of 14 and 16 mmol L^{-1} h^{-1}, resulting in CDW values that are 0.1 to 0.2-fold lower than for NH_4Cl. The additional peak observed in the approach with NH_4NO_3 could potentially indicate the shift from NH_4^+ to NO_3^- utilization after NH_4^+ was depleted. Similarly, the peak in the experiment with urea (as nitrogen source) might be attributed to a change in urea uptake. Previous studies with *P. aeruginosa* suggested an energy-dependent urea uptake system that is repressed and derepressed based on NH_4^+ availability [74–76]. In contrast, the lowest μ_{max} (0.13 h^{-1}) was

observed with $NaNO_3$, resulting in the lowest CDW of 1.2 g L^{-1}. This observation could be linked to the energy-consuming uptake and conversion of NO_3^- to NO_2^- and subsequently to NH_4^+ [14]. After reaching the OTR_{max}, all cultivations showed a flattening or slight decrease in the OTR, which might be attributed to inhibition caused by the increased pH value due to acetate consumption towards the end of the cultivation [35]. Carbon depletion is indicated by the sharp decrease shortly after.

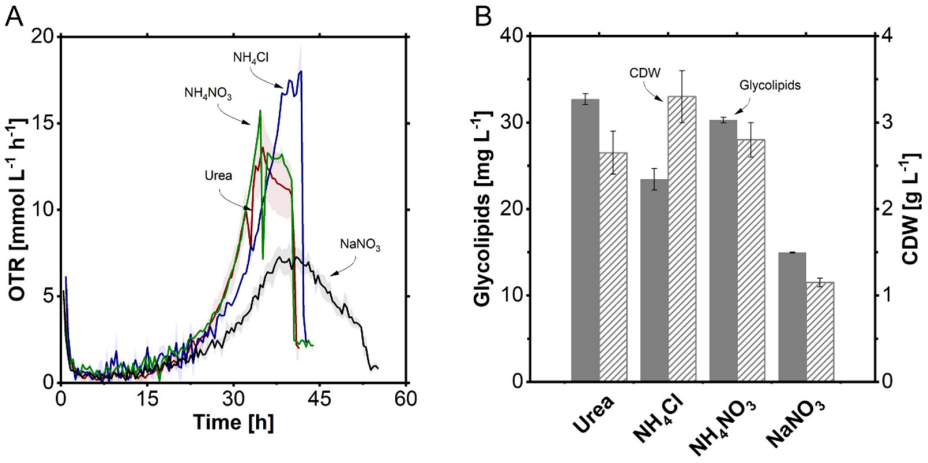

Figure 2. TOM cultivation of *A. borkumensis* SK2 with four different nitrogen sources. (**A**) Time course of oxygen transfer rate (OTR); (**B**) glycolipid concentration (filled) and cell dry weight (CDW, shaded) at the end of the cultivation. Cultivation conditions: modified ONR7a with 10 g L^{-1} acetate and equimolar nitrogen concentration of urea (red), NH_4Cl (blue), NH_4NO_3 (green), and $NaNO_3$ (black) (C/N = 8.9 Cmol $Nmol^{-1}$), N = 300 rpm, T = 30 °C, OD_{start} = 0.2, n = 2.

A. borkumensis produced the highest amount of 33 mg L^{-1} glycolipid with urea as a nitrogen source, with a 1.4-fold increase compared to NH_4Cl with 23 mg L^{-1}, which is also reflected in the highest product-to-biomass yield ($Y_{P/X}$) and highest STY of 3.3 mg g^{-1} and 0.8 mg L^{-1} h^{-1}, respectively (Figure 2B). The NH_4NO_3 approach showed similarly improved productivity, although slightly lower than with urea. The improved glycolipid production can also be explained by the more cumbersome metabolism of urea and NO_3^-, which leads to lower biomass production but higher glycolipid production. The complex uptake and metabolism processes involved in utilizing urea and NO_3^- as nitrogen sources could result in a slower metabolization of these nitrogen sources, thereby mimicking nitrogen-limiting conditions within the cell [14,30]. In contrast, NH_4^+ can be metabolized directly into biomass [14]. $NaNO_3$ revealed a glycolipid titer of 15 mg L^{-1} with the lowest STY of 0.3 mg L^{-1} h^{-1} but the highest $Y_{P/X}$ due to the low biomass. The approaches with urea, NH_4Cl, and NH_4NO_3 showed the same volumetric substrate uptake rate (r_s) of 0.24 g L^{-1} h^{-1}, while $NaNO_3$ had a lower r_s of 0.19 g L^{-1} h^{-1} due to the lower biomass concentration.

In summary, improved productivity was observed with the nitrogen sources urea and NH_4NO_3 compared to NH_4Cl and $NaNO_3$. Since urea showed a slight improvement in all parameters related to productivity and is a cheap feedstock, we decided to proceed with urea as the nitrogen source in a DO-based fed-batch fermentation. The use of carbon from urea was excluded in additional experiments.

3.2.2. Urea in DO-Based Fed-Batch Improves Glycolipid Production

The fed-batch fermentation started with 5 g L^{-1} acetate and 1.1 g L^{-1} urea. The fermentation was conducted for 60 h. After 30 h, when the acetate was depleted, DO-based feeding was initiated.

After a short lag phase, the OTR_{max} reached approximately 12 mmol L^{-1} h^{-1}, while the CDW reached 1.3 g L^{-1} with a μ_{max} of 0.14 h^{-1}, both lower than in the fermentation with NH_4Cl (Figure S3A–C). Comparing the glycolipid production during the batch phase

(23 mg L^{-1}) to the fermentation with NH_4Cl (2 mg L^{-1}), it was observed that *A. borkumensis* produced 11-fold more glycolipids. The acetate depletion occurred 4 h later than with NH_4Cl, which was attributed to the faster metabolism of NH_4^+. In contrast, urea metabolization requires the enzyme urease, which cleaves urea into NH_4^+ and CO_2. Moreover, urea uptake can occur via facilitated diffusion and actively with ATP consumption [74,75]. The specific mechanisms recruited by *A. borkumensis* remain unclear. There was an oscillatory increase in both OTR and CTR due to DO fluctuations, resulting in an OTR_{max} of 40 mmol L^{-1} h^{-1}, comparable to the cultivation with NH_4Cl. Also, the CDW increase was comparable to the cultivation with NH_4Cl, which yielded a CDW of 21 g and a 1.1-fold higher $Y_{X/S}$ of 0.38 g g^{-1} at the end of the cultivation. As the biomass increased, *A. borkumensis* produced more glycolipids, resulting in a 1.2-fold increase to 266 mg, a 1.3-fold higher $Y_{P/S}$ of 5 mg g^{-1}, and a 1.1-fold higher $Y_{P/X}$ of 13 mg g^{-1} compared to the fed-batch with NH_4Cl (Table 4). Additionally, the improved performance was supported by a 1.1-fold higher STY of 3 mg L^{-1} h^{-1} compared to the experiment with NH_4Cl. No nitrogen limitation was present, as indicated by the NH_4^+ concentration (Figure S4A). Apparently, *A. borkumensis* can efficiently take up urea, which is subsequently hydrolyzed into NH_4^+ and CO_2, as observed previously for *P. aeruginosa* [74].

Overall, the cultivation with urea showed fermentation kinetics comparable to the fermentation with NH_4Cl, with a slight improvement in productivity and glycolipid amount. Since the previous improvement in the shake flask was also evident in the DO-based fed-batch fermentation, further optimization steps were initiated to optimize the process.

3.3. Alteration in Nitrogen Availability Leads to Improved Glycolipid Production

Following urea as the preferred nitrogen source for glycolipid production, several C/N ratios were explored through shake flask experiments. In a recent study on *A. borkumensis* [18], batch fermentations showed that an NH_4Cl concentration of 2 g L^{-1} is sufficient for the consumption of 10 g L^{-1} acetate to be nitrogen-unlimited for the entire cultivation, which corresponds to a C/N ratio of 5 $g_{Acetate}$ $g_{NH4Cl}{}^{-1}$ or on a molar base 8.9 Cmol $Nmol^{-1}$. Since it is known that nitrogen-limiting conditions are advantageous for secondary metabolites, the C/N ratio was successively increased to cover a certain range. The insights gained from these trials were subsequently applied to DO-based fed-batch fermentations, where further optimization of the feeding strategy was carried out.

3.3.1. Increasing C/N Ratio Enhances Glycolipid Production

In TOM cultivation, the C/N ratios 8.9, 17.8, 26.7, 35.6, and 53.7 Cmol $Nmol^{-1}$ were tested with 10 g L^{-1} acetate and the corresponding amount of urea. As some approaches with higher C/N ratios still had half of the acetate remaining after 60 h of cultivation, the experiment was repeated in shake flasks with modifications: the acetate concentration was reduced to 5 g L^{-1} to shorten the cultivation time and mitigate the pH increase.

The overall pattern of the OTR was found to be similar among the five different C/N ratios tested (Figure 3A). Notably, the culture with the C/N ratio of 8.9 Cmol $Nmol^{-1}$ did not exhibit nitrogen limitation, and the OTR declined rapidly after 40 h due to the depletion of the carbon source. For the C/N ratios ranging from 17.8 to 53.6 Cmol $Nmol^{-1}$, a consistent trend emerged with a sudden drop in OTR after reaching its maximum. This drop occurred earlier and with a diminishing maximum as the C/N ratio increased. Subsequently, a gradual decline in the OTR was observed. As the C/N ratio increased, the onset of nitrogen limitation occurred earlier, leading to a rapid reduction in the OTR. Following this, the metabolization of acetate was reduced, resulting in lower OTR values.

Furthermore, the trend observed in the OTR was consistent with the concentration of the CDW in the shake flask experiment (Figure 3B). The final CDW decreased with increasing C/N ratio, ranging from 1.7 g L^{-1} (C/N 8.9) to 0.4 g L^{-1} (C/N 53.4). Furthermore, with a higher C/N ratio, a longer cultivation duration and slower acetate consumption were observed, with 2.5 g L^{-1} acetate left after 74 h for the C/N ratio of 53.4. This indicated that the acetate would likely not have been entirely consumed, given that active acetate

uptake is reduced in response to nitrogen-limiting conditions to conserve energy and nitrogen reserves [44,77].

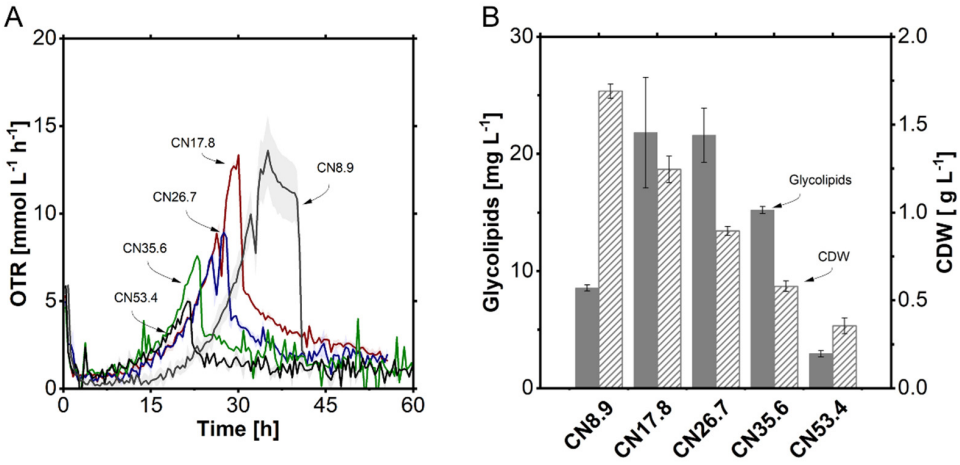

Figure 3. TOM and shake flask cultivation of *A. borkumensis* with five different C/N ratios. (**A**) Time course of OTR in TOM cultivation, specific cultivation conditions: modified ONR7a + 10 g L^{-1} acetate. (**B**) Glycolipid concentration and CDW at the end of the shake flask cultivation, specific cultivation conditions: modified ONR7a + 5 g L^{-1} acetate. Overall conditions: different C/N ratios (Cmol $Nmol^{-1}$) of urea with unchanged acetate concentration, N = 300 rpm, T = 30 °C, OD_{start} = 0.2, n = 2.

Across the various C/N ratios, *A. borkumensis* produced 9 mg L^{-1} glycolipids (Figure 3B), with a C/N ratio of 8.9 Cmol $Nmol^{-1}$. Notably, the glycolipid titer achieved with this C/N ratio was 40% of the concentration obtained with 10 g L^{-1} acetate (Section 3.2.1). This difference could potentially be attributed to altered carbon fluxes resulting from changes in carbon concentration. With increasing C/N ratio, nitrogen starvation started earlier and a higher glycolipid production was observed, but no further improvement was observed beyond a C/N ratio of 26.7 Cmol $Nmol^{-1}$. At a C/N ratio of 17.8 Cmol $Nmol^{-1}$, a 2.5-fold higher glycolipid titer (22 mg L^{-1}) was attained compared to the C/N ratio of 8.9 Cmol $Nmol^{-1}$. The C/N ratio of 26.7 Cmol $Nmol^{-1}$ achieved a similar glycolipid titer of 22 mg L^{-1} but exhibited a 1.4-fold higher $Y_{P/X}$ of 24 mg g^{-1} compared to the C/N ratio of 17.8 Cmol $Nmol^{-1}$ due to the lower CDW. The reduced glycolipid production may be due to the limiting effect of nitrogen availability beyond a C/N ratio of 26.7 Cmol $Nmol^{-1}$, which results in slower acetate uptake, leading to decreased biomass production and consequently reduced biocatalyst for glycolipid production. Additionally, pH inhibition may have played a role, as the sharp increase in pH above 8.5 could not be effectively mitigated by reducing the acetate concentration.

In summary, the investigation revealed that raising the C/N ratio led to an augmentation in glycolipid production, peaking at around 26.7 Cmol $Nmol^{-1}$. The approaches employing C/N ratios of 17.8 and 26.7 Cmol $Nmol^{-1}$ demonstrated the highest productivities, and thus, these were selected for subsequent fed-batch fermentations.

3.3.2. A Higher C/N Ratio in the Feed Increases Glycolipid Amount but Leads to Acetate Accumulation

A DO-based fed-batch fermentation with a C/N ratio of 17.8 Cmol $Nmol^{-1}$ was conducted and compared to the benchmark experiment with a C/N ratio of 8.9 Cmol $Nmol^{-1}$ (Section 3.2.2). The total duration of the fed-batch was 74 h. The feeding phase with a constant C/N ratio of 17.8 Cmol $Nmol^{-1}$ in the feed started after 29 h.

During the first 9.5 h of cultivation of the fed-batch phase, the DO fluctuated between 15% and 75%, as depicted in Figure 4B, due to oscillations between acetate depletion and consumption. After 38 h, plateaus in the DO signal were observed at a DO of 65%, resulting in reduced feeding events and a flattening of the total fed acetate after 41 h (Figure 4A,B).

The DO profile was correlated with the OTR, CTR, and CDW, all of which increased with fluctuations due to DO oscillations until 40 h. Subsequently, there was a decrease in OTR and CTR and a flattened increase in CDW, coinciding with plateau formation after 40 h. This flattened growth could be attributed to nitrogen-limiting conditions, as both urea (Figure 4C) and NH_4^+ (Figure S4B) were not detectable in the bioreactor after 38 h. Although new nitrogen was introduced with each feed event, it was quickly consumed, leading to a period with limited nitrogen in the bioreactor until the next feeding event. In response to the rare feeding events, the DO limit for feeding was lowered from 70% to 60% after 52 h, increasing OTR and CDW as more acetate and urea were fed. At 68 h, a maximum CDW of 10 g was achieved. *A. borkumensis* displayed 0.5-fold lower biomass formation under nitrogen-limiting conditions than the urea benchmark fermentation with a C/N ratio of 8.9 Cmol Nmol^{-1} (Table 4). Nitrogen depletion after 38 h resulted in less acetate consumption, leading to acetate accumulation. Lowering the DO limit contributed to the acetate accumulation until the feed was depleted after 66 h, leaving 9 g of acetate unconsumed. This can be explained by the fact that the substrate uptake rate of acetate decreases sharply under nitrogen limitation [44,77], which was also observed in the TOM shake flask cultivation (Section 3.3.1). Despite the flattened growth in biomass, *A. borkumensis* produced more glycolipids under nitrogen-limiting conditions. At the end of cultivation, the glycolipid production reached a 1.5-fold higher amount of 403 mg, with a 3-fold higher $Y_{P/X}$ of 39 mg g^{-1} and a 1.8-fold increase in $Y_{P/S}$ of 9 mg g^{-1} compared to the benchmark fed-batch fermentation with urea (Table 4). The STY was only 1.2-fold improved, reaching 4 mg L^{-1} h^{-1} due to the extended cultivation time.

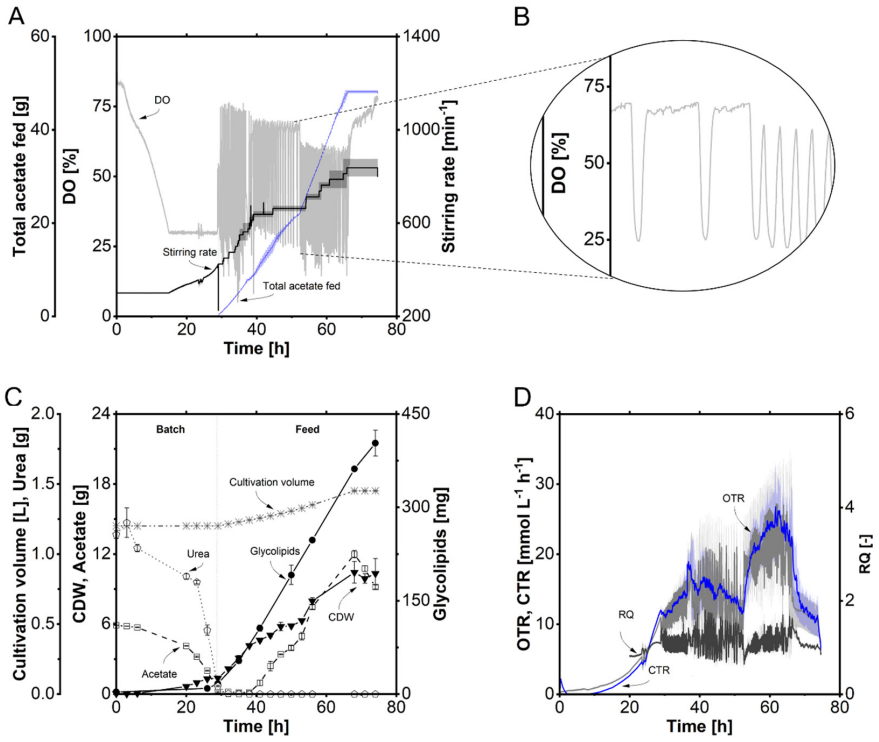

Figure 4. DO-based fed-batch fermentation of *A. borkumensis* SK2 with bubble aeration and feed with C/N of 17.8. Time course of (**A**) total acetate fed, dissolved oxygen (DO), and stirring rate; (**B**) zoom of DO between 50 and 53 h; (**C**) cultivation volume, cell dry weight (CDW), acetate, ammonium, and glycolipids amount. (**D**) Oxygen transfer rate (OTR), carbon dioxide transfer rate (CTR), and respiratory quotient (RQ). Error bands/bars indicate deviation from the mean (n = 2). Cultivation conditions: modified ONR7a medium, 3 L stirred-tank bioreactor, T = 30 °C, pH = 7.3, N = 300–1200 min^{-1} (cascaded), DO = 30%, F_{Air} = 0.41 L min^{-1}, OD_{start} = 0.2, V_L = 1.2 L. DO-based feed with C/N of 17.8 Cmol Nmol^{-1}: 200 g L^{-1} acetate, 11.2 g L^{-1} urea, 9.2 g L^{-1} NaH_2PO_4 2 H_2O, V_{Feed} = 250 mL.

The fed-batch results confirmed that a C/N ratio of 17.8 Cmol Nmol^{-1} resulted in less biomass production and increased glycolipid production, as observed in the shake flask experiments. However, acetate accumulation was observed, the prevention of which was attempted in the subsequent experiment with a two-stage feed strategy.

3.3.3. Two-Stage Feed Strategy Eliminates Acetate Accumulation

A two-stage feed strategy was implemented to address acetate accumulation observed in the fed-batch fermentation with a C/N ratio of 17.8 Cmol Nmol^{-1}. After the batch phase followed the same protocol as the previous fermentation, at 30 h, half of the acetate was fed with a C/N ratio of 8.9 Cmol Nmol^{-1} to promote biomass generation without nitrogen-limiting conditions. Subsequently, at 49 h, the first 125 mL feed containing 25 g of acetate with a C/N ratio of 8.9 Cmol Nmol^{-1} was depleted. The second feed stage started at 49 h, where the remaining 125 mL feed with 25 g of acetate with a C/N ratio of 17.8 Cmol Nmol^{-1} was fed to enhance glycolipid production. This two-stage feed approach aimed to avoid excessive acetate accumulation, which is not economically and ecologically favorable, as it represents an unused valuable resource.

At 30 h, acetate depletion led to a rapid increase in DO to over 70%, signaling the initiation of the first feed with a C/N ratio of 8.9 Cmol Nmol^{-1} (Figure 5A). Linear growth was observed, evident from the continuous increase in CDW and OTR, reaching values of 8 g and 31 mmol L^{-1} h^{-1}, respectively (Figure 5B,C). The glycolipid amount increased to 174 mg during this initial feed phase. At 49 h, the first feed was depleted, and the feed with a C/N ratio of 17.8 Cmol Nmol^{-1} was introduced. Subsequently, at 56 h, plateau formation in the DO was observed due to nitrogen-limiting conditions, prompting the reduction in the DO limit to 60%. The OTR_{max} was 39 mmol L^{-1} h^{-1} after 53 h and decreased afterward. Lowering the DO appeared to mitigate the decrease in OTR for a short period. The total acetate fed and the cultivation volume exhibited an almost linear increase until 60 h, when the second feed was depleted. An acetate accumulation of 2 g was observed after 59 h but consumed within 4 h. After 59 h, the maximum CDW of 15 g was reached with a 1.3-fold increased $Y_{X/S}$ of 0.28 g g^{-1} compared to the one-stage feed strategy with a C/N ratio of 17.8 (Table 4). Consequently, the combination of two feeds resulted in a lower CDW compared to the benchmark experiment with a C/N ratio of 8.9 Cmol Nmol^{-1} but higher than the one-stage feed strategy with a C/N ratio of 17.8 Cmol Nmol^{-1}, as expected. By 56 h, both urea and NH_4^+ were absent in the bioreactor (Figure S4C). The glycolipid production exhibited a steeper slope, with the second feed under nitrogen-limiting conditions, reaching a glycolipid amount of 377 mg at the end. Accounting for the deviation, the glycolipid production was slightly lower than in the one-stage feed strategy, with a C/N ratio of 17.8 Cmol Nmol^{-1} (403 mg). However, a 1.4-fold improvement in $Y_{P/S}$ of 7 mg g^{-1} and a 2-fold increase in $Y_{P/X}$ of 26 mg g^{-1} were achieved compared to the benchmark approach with a C/N ratio of 8.9 Cmol Nmol^{-1} (Table 4). The STY of 4 mg L^{-1} h^{-1} was 1.4-fold higher than in the benchmark approach. Intense foaming was observed after 68 h, which could have contributed to the reduced CDW and slightly flattened glycolipid production, as foaming might have extracted biomass from the fermentation broth (Figure 5D). A total of 12 g of antifoaming agent was added to counteract the strong foaming. The two-stage fed-batch was also carried out with the higher C/N ratio of 26.7 Cmol Nmol^{-1} to compare the two higher C/N ratios in the fed-batch.

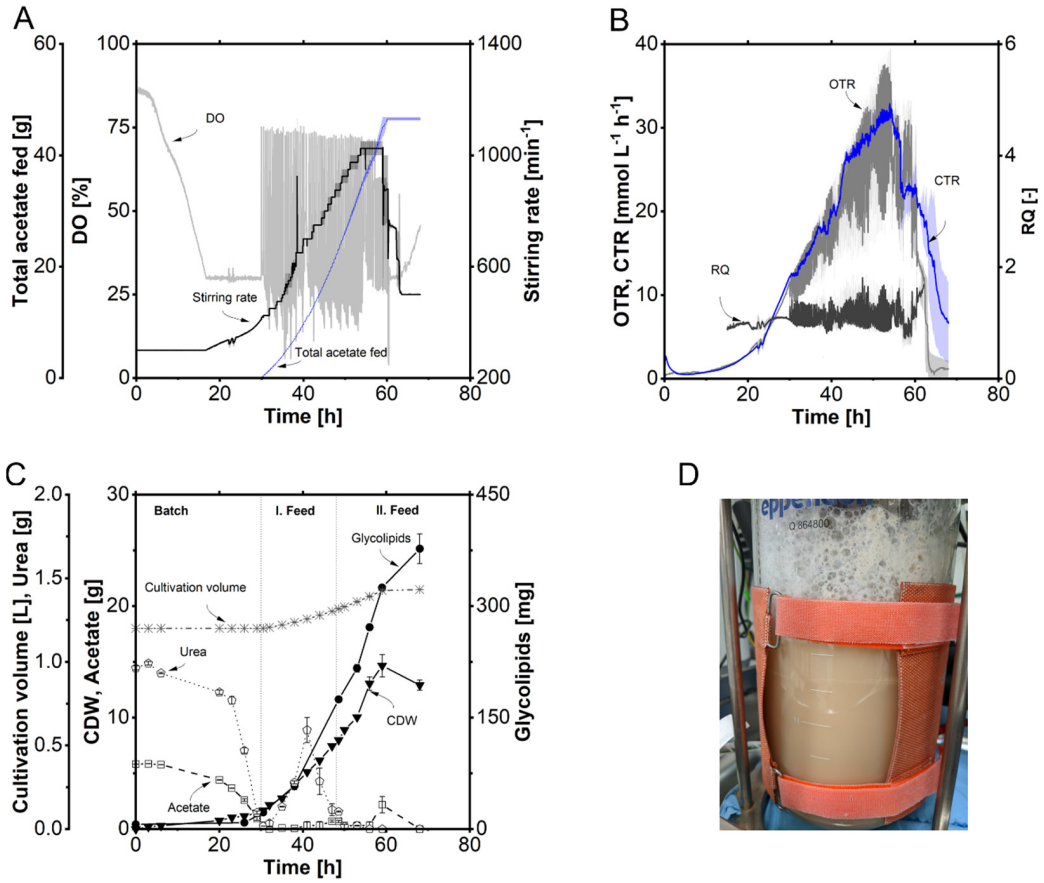

Figure 5. DO-based fed-batch fermentation of *A. borkumensis* SK2 with bubble aeration and a two-stage feed strategy with C/N of 17.8. Time course of (**A**) total acetate fed, dissolved oxygen (DO), and stirring rate; (**B**) oxygen transfer rate (OTR), carbon dioxide transfer rate (CTR), and respiratory quotient (RQ); (**C**) cultivation volume, cell dry weight (CDW), acetate, ammonium, and glycolipid amount. (**D**) Foto of the formed foam in the bioreactor after 68 h cultivation. Error bands/bars indicate deviation from the mean (n = 2). Cultivation conditions: modified ONR7a medium, 3 L stirred-tank bioreactor, T = 30 °C, pH = 7.3, N = 300–1200 min^{-1} (cascaded), DO = 30%, F_{Air} = 0.41 L min^{-1}, OD_{start} = 0.2, V_L = 1.2 L. First DO-based feed with C/N of 8.9 Cmol $Nmol^{-1}$: 200 g L^{-1} acetate, 22.4 g L^{-1} urea, 9.2 g L^{-1} NaH_2PO_4 2 H_2O, V_{Feed} = 125 mL. Second DO-based feed with C/N of 17.8 Cmol $Nmol^{-1}$: 200 g L^{-1} acetate, 11.2 g L^{-1} urea, 9.2 g L^{-1} NaH_2PO_4 2 H_2O, V_{Feed} = 125 mL.

3.3.4. Too High C/N Ratio Leads to Acetate Accumulation Even with the Two-Stage Feed Strategy

Since the C/N ratio of 26.7 Cmol $Nmol^{-1}$ in the preliminary test had the highest titers besides 17.8, this C/N ratio was also tested in the two-stage fed-batch. The two-stage feed strategy with a C/N ratio of 26.7 Cmol $Nmol^{-1}$ was examined for a total duration of 71 h, following the procedures described in Section 3.3.3. The first feed with a C/N ratio of 8.9 Cmol $Nmol^{-1}$ was initiated after 32 h, while the second feed with a C/N ratio of 26.7 Cmol $Nmol^{-1}$ started after 49 h.

After 49 h, the first feed was depleted with a comparable CDW of 8 g and glycolipid amount of 186 mg, after which the second feed started with a C/N ratio of 26.7 Cmol $Nmol^{-1}$ (Figure 6A,C). Due to the higher C/N ratio, plateau formation in DO occurred 3 h earlier (at 53 h) compared to the experiment in Section 3.3.3, leading to no further increase in the stirring rate beyond 1000 min^{-1}. The DO limit was lowered to 60%, resulting in a steady DO oscillation between 33% and 60%. These oscillations were no longer due to acetate depletion but, instead, to a lack of nitrogen source, which is evident from the depletion of urea and NH_4^+ (Figure S4D) after 53 h. Nitrogen-limiting conditions caused a flattening of CDW and acetate accumulation. The OTR_{max} peaked at

approximately 37 mmol L^{-1} h^{-1} after about 52 h, followed by a decrease due to plateau formation (Figure 6B). At around 59 h, the entire feed was exhausted, rapidly decreasing OTR and CTR. Until the feed was depleted, 7 g of acetate accumulated, and the maximum CDW reached 16 g. All acetate was depleted after 71 h, and the CDW slightly decreased to 13 g. The CDW was only slightly lower compared to the two-stage feed strategy with a C/N ratio of 17.8 Cmol $Nmol^{-1}$, suggesting that the first feed with a C/N ratio of 8.9 Cmol $Nmol^{-1}$ was responsible for most of the growth (Table 4). The relatively high nitrogen content in the first feed allowed for NH_4^+ accumulation until the end of the first feed, enabling further growth during the second feed.

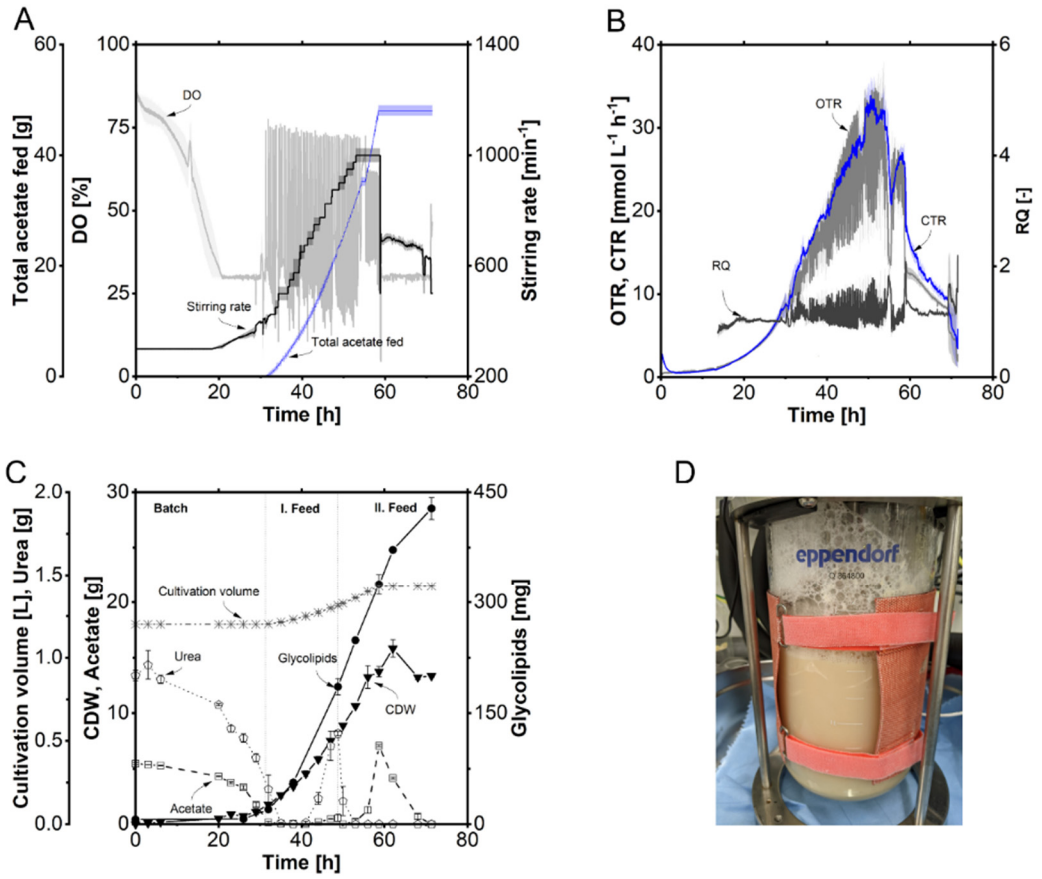

Figure 6. DO-based fed-batch fermentation of *A. borkumensis* SK2 with bubble aeration and a two-stage feed strategy with C/N of 26.7. Time course of (**A**) total acetate fed, DO, and stirring rate; (**B**) oxygen transfer rate (OTR), carbon dioxide transfer rate (CTR), and respiratory quotient (RQ); (**C**) cultivation volume, CDW, acetate, ammonium, and glycolipid amount. (**D**) Foto of the formed foam in the bioreactor after 71 h cultivation. Error bands/bars indicate deviation from the mean (n = 2). Cultivation conditions: modified ONR7a medium, 3 L stirred-tank bioreactor, T = 30 °C, pH = 7.3, N = 300–1200 min^{-1} (cascaded), DO = 30%, F_{Air} = 0.41 L min^{-1}, OD_{start} = 0.2, V_L = 1.2 L. First DO-based feed with C/N of 8.9 Cmol $Nmol^{-1}$: 200 g L^{-1} acetate, 22.4 g L^{-1} urea, 9.2 g L^{-1} NaH_2PO_4 2 H_2O, V_{Feed} = 125 mL. Second DO-based feed with C/N of 26.7 Cmol $Nmol^{-1}$: 200 g L^{-1} acetate, 7.5 g L^{-1} urea, 9.2 g L^{-1} NaH_2PO_4 2 H_2O, V_{Feed} = 125 mL.

Overall, the two-feed strategy with a C/N ratio of 26.7 Cmol $Nmol^{-1}$ increased the glycolipid amount by 1.1-fold to 428 mg, compared to the two-feed strategy with a C/N of 17.8 Cmol $Nmol^{-1}$ experiment at the end of cultivation (Table 4). With a total duration of 71 h, this fermentation lasted 8 h longer than the two-stage feed strategy with a C/N ratio of 17.8 Cmol $Nmol^{-1}$. Foam formation (Figure 6D) was difficult to control after 71 h due to the formation of stable foam. In total, 9 g of the antifoaming agent was used.

In summary, employing the two-stage feed strategy in the experiments resulted in favorable productivity while avoiding excessive acetate accumulation. The comparable STY indicates a constraint on further productivity improvement through the C/N ratio, in line with the findings from the preliminary experiments (Section 3.3.1). Given that a C/N ratio of 26.7 Cmol $Nmol^{-1}$ led to increased cultivation time, the subsequent experiment focused solely on investigating the C/N ratio of 17.8 Cmol $Nmol^{-1}$.

3.4. pH-Stat Fed-Batch Fermentation for Optimized Glycolipid Production

An alternative approach was explored to overcome the limitations posed by reaching the maximum acetate solubility in the regular feed and considering that increasing the feed volume might lead to product dilution. This involved introducing additional carbon into the system using glacial acetic acid, a method already investigated in growth experiments with *C. glutamicum* [43,44]. The rationale behind this approach lies in the fact that acetate consumption leads to an increase in the pH of the culture medium due to the removal of equimolar protons and acetate. Glacial acetic acid was introduced into the system to address this rise in pH, and the feeding rate was controlled based on microbial growth kinetics. Specifically, the glacial acetic acid addition rate was correlated with the current microbial acetate uptake rate, as the pH increase correlates with the acetate uptake rate [43]. In the subsequent fed-batch fermentation, a combination of an acetate feed with a C/N ratio of 8.9 Cmol $Nmol^{-1}$ and a pH-coupled feed with glacial acetic acid using the C/N ratio of 17.8 Cmol $Nmol^{-1}$ was tested. The batch was initially operated in the same manner as in the previous experiments, utilizing 4 M H_2SO_4 as the pH agent. At the beginning of the fed-batch phase, a total of three to four pulses of acetate feed at a C/N ratio of 8.9 Cmol $Nmol^{-1}$ was fed to ensure adequate biomass formation and to provide sufficient carbon to the system in case the acetic acid titration was insufficient.

3.4.1. pH-Stat Fed-Batch Process—A Highly Optimized Process with Bubble Aeration

The pH-stat fed-batch process had a starting volume of 1.2 L. With the acetate depletion after 32 h, the feeding phase was started by switching from H_2SO_4 to glacial acetic acid containing urea with a C/N ratio of 17.8 Cmol $Nmol^{-1}$. To prevent carbon limitation, which was indicated by an increase in DO and decrease in stirring rate, 2.4 g and 1.2 g of acetate with a C/N ratio of 8.9 Cmol $Nmol^{-1}$ were introduced after 32, 34, 39, and 46 h, respectively (indicated with the star symbol in Figure 7C). The experiment resulted in an increased OTR_{max} of 50 mmol L^{-1} h^{-1} after 57 h (Figure 7B). The continuous nitrogen addition achieved through glacial acetic acid titration allowed for a sustained nitrogen supply, unlike the previous experiments with the two-stage feed strategy. The cultivation demonstrated a steady CDW increase during the feed phase, reaching a maximum of 14 g, comparable to fermentations with the two-stage feed strategy (Figure 7C) (Table 4). Urea was depleted after 38 h, and NH_4^+ was exhausted after 47 h (Figure S4E). The acetate accumulation stabilized at around 5 g at the beginning of the feed phase and remained constant throughout the cultivation period. Approximately 3 g of acetate persisted at the end of fermentation, with 59 g fed, and about 56 g of acetate was metabolized during the feed phase. A constant cultivation volume of 1.2 L was maintained over the entire period since the undiluted glacial acetic acid was directly metabolized, in contrast to the acetate feed in the DO-based fed-batch fermentations, which mainly consisted of water, leading to medium dilution. Foaming was relatively low compared to all other fermentations (Figure 7D). In total, only 3 g of the antifoaming agent was added. This may be due to the constant filling volume and the lower stirrer speed than the other fermentations.

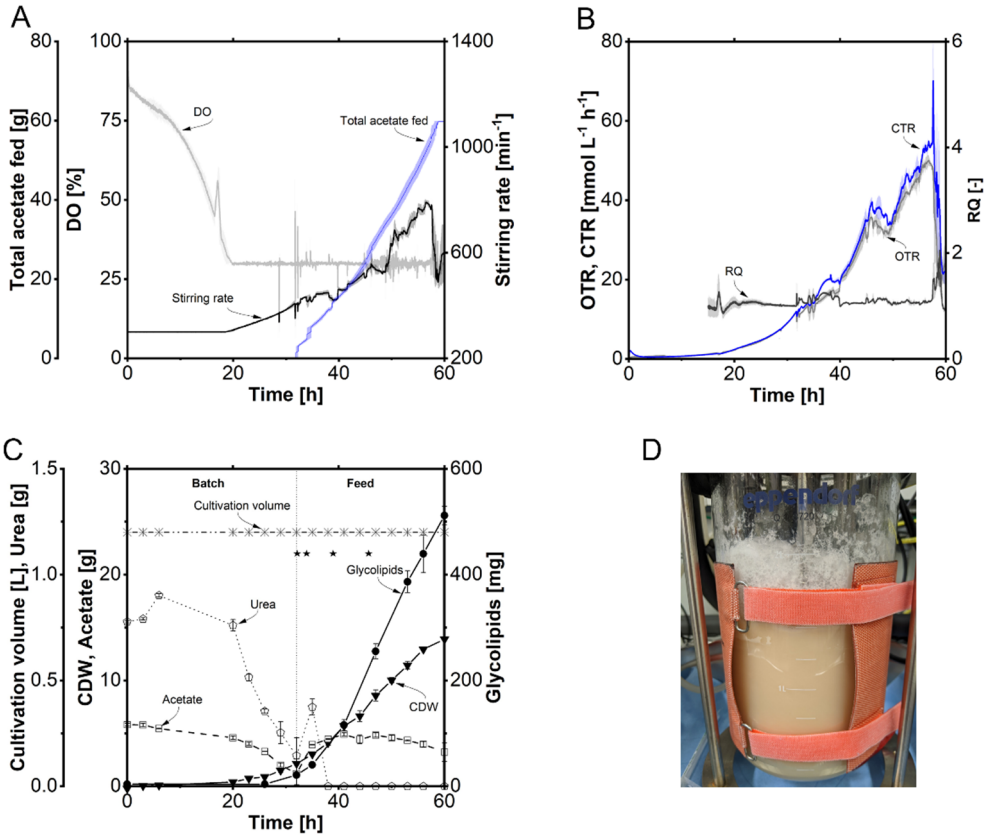

Figure 7. pH-stat fed-batch fermentation of *A. borkumensis* SK2 with bubble aeration and glacial acetic acid with C/N of 17.8 as feed. Time course of (**A**) total acetate fed, DO, and stirring rate; (**B**) oxygen transfer rate (OTR), carbon dioxide transfer rate (CTR), and respiratory quotient (RQ); (**C**) cultivation volume, CDW, acetate, urea, and glycolipid amount with (★) = acetate pulse with C/N 8.9 Cmol Nmol^{-1}. (**D**) Foto of the formed foam in the bioreactor after 60 h cultivation. Error bands/bars indicate deviation from the mean (n = 2). Cultivation conditions: modified ONR7a medium, 3 L stirred-tank bioreactor, T = 30 °C, pH = 7.3, N = 300–1200 min^{-1} (cascaded), DO = 30%, F_{Air} = 0.41 L min^{-1}, OD_{start} = 0.2, V_L = 1.2 L. Glacial acetic acid feed with C/N of 17.8 Cmol Nmol^{-1}: 1050 g L^{-1} acetic acid, 59.0 g L^{-1} urea, 24.2 g L^{-1} NaH_2PO_4 2 H_2O, V_{Feed} = 50 mL.

A. borkumensis demonstrated the highest glycolipid production through the glacial acetic acid feed compared to previous experiments, yielding 512 mg. Despite utilizing 6 g more acetate, the $Y_{P/S}$ increased by 1.1-fold, and the $Y_{P/X}$ was 1.4-fold higher compared to the two-feed strategy with a C/N ratio of 17.8 Cmol Nmol^{-1}. The STY reached 7 mg L^{-1} h^{-1}, the highest among all the experiments (Table 4).

3.4.2. Membrane Aeration in pH-Stat Fed-Batch Sustains Foam-Free Fermentation without Performance Loss

The optimized conditions of the pH-stat fed-batch fermentation from the previous section were subsequently used with a bubble-free membrane aeration module to avoid foaming and the resulting antifoaming agent addition. With a duration of 59 h, the membrane-aerated ph-stat fed-batch process had an increased starting volume of 2.0 L. The feeding phase with a constant C/N ratio of 17.8 Cmol Nmol^{-1} started after 41 h.

The batch process lasted 9 h longer than the bubble-aerated process (Section 3.4.1). During the experiment, acetate depletion was apparent, as indicated by the increase in DO of over 70% (Figure 8A,C). As in the bubble-aerated process, 2.4 g of acetate was added directly with a C/N ratio of 8.9 Cmol Nmol^{-1}, and the acid titration method was switched from H_2SO_4 to glacial acetic acid containing urea with a C/N ratio of 17.8 Cmol Nmol^{-1}. Subsequently, additional pulses of 2.4 g acetate were added after 45 h and 50 h, respectively

(indicated with the star symbol in Figure 8C). The experiment resulted in an increased CO_2 signal in the off-gas of 4% after 58 h compared to the benchmark membrane process with 3% (Section 3.1.2). Pure oxygen in the supply gas was added up to a share of 90% until the end of the process to supply the process with sufficient oxygen (Figure 8A). The cultivation showed a steady CDW increase during the feeding phase, reaching a maximum of 17 g with a $Y_{X/S}$ of 0.27 g g^{-1}, 1.2-fold higher than the bubble-aerated process (Table 4). Urea was depleted after 53 h. Acetate accumulation stabilized at about 4 g at the beginning of the feeding phase and remained constant throughout the cultivation period. At the end of fermentation, about 4 g of acetate was still present, 59 g was fed, and 54 g of acetate was metabolized during the feeding phase. Membrane aeration completely prevented foam formation, and no antifoaming agent was added (Figure 8D).

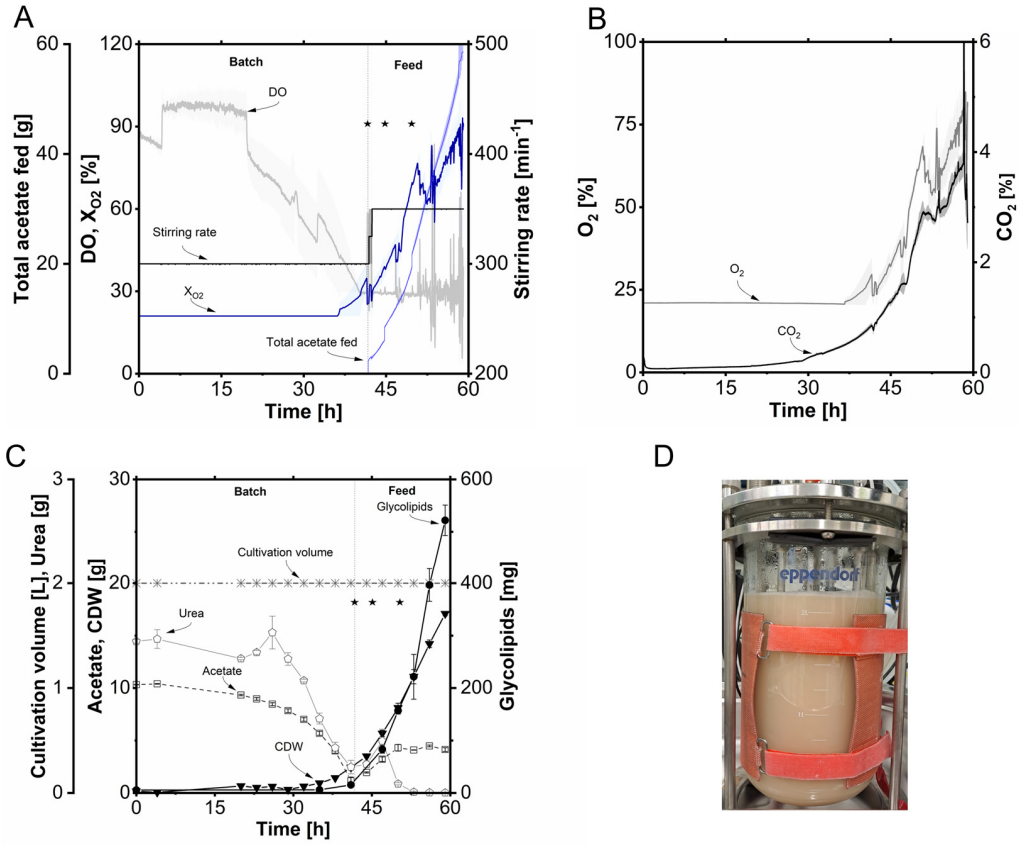

Figure 8. pH-stat fed-batch fermentation of *A. borkumensis* SK2 with bubble-free membrane aeration and glacial acetic acid with C/N of 17.8 as feed. Time course of (**A**) total acetate fed, DO, X_{O2}, and stirring rate; (**B**) O_2 and CO_2 concentration in the off-gas; (**C**) cultivation volume, cell dry weight (CDW), acetate, ammonium, and glycolipid amount with (★) = acetate pulse with C/N 8.9 Cmol $Nmol^{-1}$. (**D**) Foto of the formed foam in the bioreactor after 56 h cultivation. Error bands/bars indicate deviation from the mean (n = 2). Cultivation conditions: modified ONR7a medium, 3 L stirred-tank bioreactor, T = 30 °C, pH = 7.3, N = 300–350 min^{-1}, DO = 30%, TMP = 0.3 bar X_{O2} = 21–100% (cascaded), F_{Gas} = 1.0 L min^{-1}, OD_{start} = 0.2, V_L = 2.0 L. Glacial acetic acid feed with C/N of 17.8 Cmol $Nmol^{-1}$: 1050 g L^{-1} acetic acid, 59.0 g L^{-1} urea, 24.2 g L^{-1} NaH_2PO_4 2 H_2O, V_{Feed} = 50 mL.

Again, the highest glycolipid production was achieved with *A. borkumensis* using this feeding strategy. The glycolipid amount produced was 521 mg, similar to the bubble-aerated process. Also, the $Y_{P/S}$ and $Y_{P/X}$ were obtained with 8 mg g^{-1} and 31 mg g^{-1}, comparable to the bubble-aerated pH-stat process (Table 4). However, the STY was 0.4-fold lower at 4 mg L^{-1} h^{-1} because the glycolipid concentration was lower due to the higher filling volume in the membrane-aerated process since it was diluted 1.6-fold.

3.5. Assessment of Glycine-Glucolipid Bioactivity against Pathogenic Bacteria

Biosurfactants often exhibit bioactivities or can support the activities of hydrophobic compounds. Early reports indicated the absence of toxic effects of *A. borkumensis*-derived glucolipids on marine microbes (Proteobacteria, flagellates, and microalgae) and erythrocytes [78,79]. The described production strategy enables the evaluation of the potential of glycine-glucolipid as an antimicrobial agent. Utilizing a serial dilution technique with a factor of two, ranging from 337 mg L^{-1} to 0.04 mg L^{-1}, we investigated the effect of glycine-glucolipid on the growth of six different bacterial strains, including the five pathogenic strains *S. marcescens*, *S. epidermidis*, *E. faecium*, *S. aureus*, and *P. aeruginosa*, and the mycobacterium *C. glutamicum* (2.5). The minimum inhibitory concentration (MIC) and half maximal inhibitory concentration (IC50) values were assessed if applicable (Table 5).

Table 5. Determination of IC50 values for various glycine-glucolipid concentrations via analysis of relative bacterial biomass. Relative biomass [%] of different bacteria achieved after 20 h in the presence of different glycine-glucolipid concentrations. The OD_{750nm} of the cultures at 0 mg L^{-1} concentration of the respective component was set as 100% relative biomass. The half maximal inhibitory concentration (IC50) was detected at a relative biomass of 50% (area marked with line). The values represent the mean of two independently conducted experiments with each carried out in triplicate (n = 2).

rel. biomass [%]	$c_{glycine\text{-}glucolipid}$ [mg·L^{-1}]	0	0.04	0.08	0.16	0.33	0.66	1.32	2.63	5.3	12	21	42	84	169	337
	C. glutamicum	100 ± 8	82 ± 10	100 ± 9	90 ± 9	96 ± 4	81 ± 2	95 ± 8	72 ± 5	52 ± 6	62 ± 4	62 ± 3	60 ± 10	64 ± 2	61 ± 1	59 ± 3
	S. marcescens	100 ± 6	87 ± 5	97 ± 2	102 ± 14	98 ± 1	95 ± 4	109 ± 12	84 ± 8	87 ± 8	63 ± 8	52 ± 10	42 ± 8	42 ± 12	32 ± 9	42 ± 10
	S. epidermidis	100 ± 9	78 ± 3	81 ± 3	82 ± 8	83 ± 4	73 ± 4	85 ± 0	93 ± 3	98 ± 3	91 ± 2	94 ± 1	104 ± 4	109 ± 7	104 ± 1	103 ± 4
	E. faecium	100 ± 8	82 ± 6	89 ± 2	91 ± 3	87 ± 1	91 ± 3	86 ± 5	78 ± 3	49 ± 2	73 ± 3	73 ± 5	43 ± 4	46 ± 9	45 ± 7	50 ± 0
	S. aureus	100 ± 2	98 ± 8	83 ± 9	92 ± 9	84 ± 0	96 ± 2	77 ± 5	92 ± 3	68 ± 7	36 ± 9	47 ± 1	51 ± 1	58 ± 2	68 ± 2	66 ± 2
	P. aeruginosa	100 ± 6	100 ± 9	92 ± 4	100 ± 7	111 ± 9	102 ± 9	122 ± 6	94 ± 6	93 ± 4	95 ± 6	77 ± 3	72 ± 2	85 ± 4	101 ± 8	104 ± 9

Interestingly, the glycine-glucolipid did not completely inhibit the growth of any investigated species, preventing the determination of MICs. Only *C. glutamicum*, *S. epidermidis*, *E. faecium*, and *S. aureus* exhibited sensitivity to the glycine-glucolipid, with effective concentrations ranging from 5.3 (*C. glutamicum*) to 43 mg L^{-1} (*E. faecium*), resulting in an up to 60% reduction in bacterial growth. For *S. marcescens* and *E. faecium*, the IC50 values of 42 mg L^{-1} were determined. To extend our understanding of glycine-glucolipid's potential, we evaluated its combinatorial effects with tetracycline and chloramphenicol using the Checkerboard survival assay method (Figure S5). Here, no effects of the biosurfactant were observed with regard to the antibiotic activity of both compounds.

4. Discussion

The use of *A. borkumensis* for biosurfactant production has spurred interest with regard to bioeconomic processes due to its ability to metabolize sustainable carbon sources like acetate [15,35]. In a previous study using acetate and NH_4Cl as carbon and nitrogen sources, *A. borkumensis* produced 43 mg L^{-1} of glycolipids in batch fermentation [18]. The study carried out here aimed to enhance the productivity of the fermentation using acetate as the sole carbon source. Different nitrogen sources were initially evaluated to achieve this, and subsequently, the best C/N ratios were investigated for optimal productivity. In the final fermentation, glacial acetic acid served as both a pH agent and an additional carbon source, allowing the introduction of more carbon without diluting the system.

The investigation of nitrogen sources revealed that changing from NH_4Cl to urea as the nitrogen source in fed-batch fermentation improved glycolipid production by at least 20%. The ability of *A. borkumensis* to metabolize urea contradicted the findings of Yakimov et al. [15]. It was deduced that the method used in the previous publication may

not have adequately tested the urease activity in *A. borkumensis*. *A. borkumensis* possibly possesses an energy-dependent urea uptake system similar to *P. aeruginosa*, regulated by nitrogen availability [74,75]. The presence of urease was observed, enabling the hydrolysis of urea into NH_4^+, which was secreted into the supernatant. A review of the database UniProt reported the subunits UreA, UreB, and UreC with their corresponding genes (ABO_2719-ABO_2721), as well as the accessory proteins UreD, UreF, and UreG (ABO_2722, ABO_2716, ABO_2715) of the urease in *A. borkumensis* [14,80].

The improved $Y_{P/X}$ on all nitrogen sources compared to NH_4Cl may be attributed to slow growth, as these substrates involve additional metabolic steps compared to NH_4Cl. NH_4^+ is taken up by facilitated diffusion and directly metabolized, whereas NO_3^- uptake requires energy and conversion to NH_4^+ via NO_2 [14]. This elaborate uptake and metabolism of urea and NO_3^- may simulate nitrogen-limiting conditions in the cell [30]. Studies with *P. aeruginosa* in shake flask experiments showed that switching to $NaNO_3$, urea or NH_4NO_3 improved rhamnolipid production compared to NH_4Cl but also resulted in lower biomass production [30,31]. However, unlike in *A. borkumensis*, the reduced biomass production by *P. aeruginosa* on $NaNO_3$ did not decrease rhamnolipid production. Nitrogen-limiting or growth-limiting conditions are known to increase the productivity of rhamnolipids, as less carbon is invested in biomass formation and secondary metabolite production is induced [3,81,82]. In the case of rhamnolipids, the sigma factor 54 RpoN, which regulates nitrogen metabolism, is responsible for the expression of *rhlABC* under these conditions [82,83].

The influence of different C/N ratios, thus nitrogen-limiting conditions, on productivity was investigated in the second part of this study. In shake flask experiments, increasing the original C/N ratio from 8.9 Cmol $Nmol^{-1}$ to 17.8 and 26 Cmol $Nmol^{-1}$ resulted in a more than threefold increase in glycolipid titer and $Y_{P/X}$. However, no further enhancement was observed beyond a C/N ratio of 26.7 Cmol $Nmol^{-1}$. It was concluded that earlier nitrogen-limited conditions directed more carbon toward glycolipid production rather than biomass production. Nonetheless, nitrogen limitation also led to slower acetate metabolism [77]. Additionally, high C/N ratios might trigger the production of storage molecules like TAG and WE, diverting carbon away from glycolipid production [20], which could contribute to the observed decrease in enhancement during the preliminary experiments. The potential for increased glycolipid production through nitrogen-limiting conditions in *A. borkumensis* was previously observed with *n*-alkanes as the carbon source [16]. Similarly, *P. aeruginosa* exhibited increased rhamnolipid titer with higher C/N ratios. However, the limitation of enhancement was observed at a C/N ratio of 62 Cmol $Nmol^{-1}$ with $NaNO_3$ as the nitrogen source and glycerol as the carbon source, and the limiting C/N ratio was found to depend on the carbon source [32]. Another factor influencing glycolipid production at high C/N ratios was demonstrated by Invally and Ju [72] in their fed-batch fermentation study of *P. aeruginosa*. They discovered that a steady, small nitrogen feed was essential to maintain cell activity for rhamnolipid production. A two-stage feed strategy was developed, involving an initial phase to achieve high cell density with sufficient nitrogen, followed by a controlled nitrogen-limiting feed phase that allowed no further growth but maintained cell activity for rhamnolipid production.

In *P. aeruginosa*, the sigma factor 54 RpoN plays a role in nitrogen metabolism [83,84]. The genes responsible for rhamnolipid production are likely indirectly or directly controlled by RpoN under nitrogen-limiting conditions, with upregulation of glutamine synthetase being involved. Increasing nitrogen assimilation through upregulation of the ATP-dependent pathway of glutamine synthetase appears to lead to higher nitrogen uptake and, consequently, an upregulation of rhamnolipid biosynthesis [84]. A similar mechanism could potentially be involved in *A. borkumensis*, as the UniProt database predicts a gene ABO_0552 of *A. borkumensis* to encode a *rpoN* homolog [80]. In this context, the upregulated ATP-dependent metabolic pathway via glutamine synthetase might also explain the observed reduction in biomass production in *A. borkumensis*.

The variation of the C/N ratios in the fermentation led to a high glycolipid amount of 403 mg with a feed of 17.8 Cmol $Nmol^{-1}$ (Table 4). However, a relatively high acetate accumulation was also observed at the end of the fermentation. High C/N ratios above 50 promote the production of storage compounds like PHA, WE, and TAG, which is undesirable [20,21]. Since glycolipids and storage compounds share the same de novo fatty acid precursor, they might be produced simultaneously [16]. Moreover, high acetate accumulation might have contributed to flattened growth by causing cytosol acidification, disrupting the proton gradient for ATP synthesis, and activating stress response genes [46,85]. Furthermore, the prolonged process duration of 74 h, with increasing difficulty in controlling foaming, had negative implications for process feasibility and STY. Kiefer et al. [43] suggested that the C/N consumption ratio can change over time during fed-batch fermentation. The authors emphasized the need to find a balance where nitrogen is neither overfed nor underfed, leading to the development of a two-stage feed strategy where the C/N ratio of the feed is adjusted to the metabolism.

In this study, a two-stage feed strategy was developed involving the addition of half of the acetate during the "growth phase" without nitrogen limitation at a C/N ratio of 8.9 Cmol $Nmol^{-1}$, followed by feeding the other half during the "production phase" with a C/N ratio of 17.8 or 26.7 Cmol $Nmol^{-1}$. This approach resulted in slightly lower glycolipid production than the one-stage feed strategy, but it effectively prevented excessive acetate accumulation, leading to higher STY than the one-stage feed strategy. While the two-stage feed approach seems promising for increasing productivity under nitrogen-limiting conditions with acetate as the carbon source, DO-based fed-batch fermentation may not be the most suitable since it can control only one limitation at a time. A fed-batch fermentation with a two-stage feed strategy involving continuously added feed, increasing with increasing growth, might be more fitting. Nevertheless, keeping the carbon concentration as low as possible is essential to avoid substrate inhibition and the production of storage components. Similar two-stage feed strategies have been successfully implemented in prior publications to enhance productivity, as seen in poly-β-hydroxybutyric acid (PHB) production with *Methylorubrum extroquens*. In that study, biomass was first produced under nitrogen-unlimited conditions, followed by PHB production in the subsequent production phase under nitrogen-limiting conditions with constant feeding with an iteratively increasing C/N ratio [86].

Last, a pH-stat fed-batch with glacial acetic acid titration was tested with a C/N ratio of 17.8 Cmol $Nmol^{-1}$ and a pulsed feeding of sodium acetate with a C/N ratio of 8.9 Cmol $Nmol^{-1}$. This continuous feed addition contributed to increased and accelerated glycolipid production. A similar two-stage feed strategy using glacial acetic acid as a carbon source and pH agent was carried out by Merkel et al. [44] for itaconate production using *C. glutamicum*. Their study initiated a "growth phase" with a C/N ratio of 10 Cmol $Nmol^{-1}$ after the batch, followed by a second feed with a C/N ratio of 40 Cmol $Nmol^{-1}$ in the "production phase". They used pH-coupled feeding with glacial acetic acid and a DO-based sodium acetate feed pulsed at 5 g L^{-1} acetate concentrations. However, unlike itaconate production, *A. borkumensis* continued to produce biomass even after the growth phase, which could be attributed to the lower C/N ratio in the second feed. In contrast, the increases in DO observed in this work, leading to the acetate feed pulses, were due to nitrogen rather than carbon limitation.

An advantage of the glacial acetic acid titration fermentation in this work was the $Y_{P/S}$, comparable to the other DO-based fed-batch fermentations (Table 4). In contrast, Merkel et al. [44] reported a disadvantage of low $Y_{P/S}$ with a glacial acetic acid titration approach. Huschner et al. [87] developed a pH-coupled fed-batch fermentation for PHA production using *Cupriavidus necator* H16, in which nitrogen was dissolved in the organic acids, similar to this study. Additionally, they added a DO-based feed without nitrogen. Their three-stage fed-batch fermentation with C/N ratios of 10 Cmol $Nmol^{-1}$, 90 Cmol $Nmol^{-1}$, and ∞ Cmol $Nmol^{-1}$ significantly improved PHA production. However, they also observed acetate accumulation starting at the C/N ratio of 90 Cmol $Nmol^{-1}$, and

the biomass decreased with the start of the limiting 90 Cmol $Nmol^{-1}$ feed. In a subsequent study, Garcia-Gonzalez and Wever [88] further optimized the PHA production of *C. necator* using the same three-stage feed strategy, with glacial acetic acid as the pH-coupled feed and sodium acetate as the DO-based feed. However, they did not observe acetate accumulation; they noted decreasing biomass when nitrogen was depleted.

The pH-coupled glacial acetic acid titration approach offered several advantages, such as feeding an autosterile medium without causing a dilution effect and reducing the salt load compared to sodium acetate [35,43,44]. However, one challenge encountered during extended feeding was the increased difficulty in controlling foam formation as the process progressed. To address this issue, bubble-free aeration with an in situ membrane module was considered in this study as a potential solution [62,63]. Membrane aeration provides growth conditions similar to bubble-aerated processes but with the advantage of eliminating foaming. As a result, there is no need for antifoaming agents, which significantly simplifies downstream processing and reduces associated costs [63]. However, the formation of biofilms on the membrane surface, the associated reduction in oxygen transfer performance, and the reusability of the membrane modules must be mentioned as disadvantages. In conclusion, the two-feed strategy using glacial acetic acid shows great promise for enhancing the glycolipid production of *A. borkumensis*. Similar approaches suggest that this strategy could be successfully applied to other organisms and products [44,87].

In contrast to other glycolipids, no pronounced antimicrobial activity of the glycine-glucolipid was observed against the tested selection of bacterial strains. A subset of bacteria exhibited sensitivity to glycine-glucolipid at concentrations exceeding 43 mg L^{-1}. Given the limited existing knowledge of the physicochemical properties of these glycine-glucolipids [17], this sensitivity at specific concentrations might suggest micelle formation, enabling subsequent growth inhibition [89–91]. The variation in sensitivity between bacterial strains may indicate different mechanisms of action, as observed in other studies that emphasized the role of bacterial cell envelope architecture in antimicrobial sensitivity [92–94]. In light of the role of *A. borkumensis* in hydrophobizing cell surfaces [25,28], it is hypothesized that glycine-glucolipid could enhance the bioavailability of rather hydrophobic antibiotics like tetracycline and chloramphenicol to the cells, thereby reducing the required antibiotic dosage as reported for other surfactant and antibiotic combinations [95,96]. However, no effects of the glycine-glucolipid on the activity of tetracycline and chloramphenicol were observed in our study. For a more comprehensive understanding of its potential for antimicrobial applications, further studies involving a broader range of antibiotics and the determination of physicochemical parameters are needed.

While our study primarily focused on the bioactivity of the glycine-glucolipid against specific pathogenic bacterial strains, the potential environmental applications should not be overlooked. For instance, the low toxicity observed suggests that glycine-glucolipids could be employed in environmental remediation projects or wastewater treatment without significantly disrupting the existing microbial communities. This aligns with earlier findings, which reported low toxicity of *A. borkumensis*-derived glucolipids on marine microbes [78,79].

5. Conclusions

In conclusion, significant improvements in glycolipid titers with *A. borkumensis* were achieved by implementing a DO-based two-stage feed strategy and using pH-stat fed-batch with glacial acetic acid titration. To achieve glycolipid production on a g L^{-1} scale with *A. borkumensis*, metabolic engineering techniques such as knockouts or overexpression could address issues such as by-product formation from storage molecules or enhance the expression of the glycolipid gene cluster. The availability of biobased-produced acetic acid from lignocellulose offers a sustainable alternative to petrochemical or food-competing substrates for glycolipid production. In the long term, CO_2 + green H_2-derived acetate from acetogens [97] will deliver acetate for a land-free biotechnology. This advancement aligns with ecological and economic goals. Regarding process technology, in situ membrane aeration effectively mitigated strong foam formation during cultivation. Furthermore, in

the bioactivity test, no noticeable antimicrobial effect was detected. This may indicate low or even missing toxicity of *A. borkumensis* glycolipid, suggesting its use in cleaning products, the food industry, and textiles, thereby offering an eco-friendly alternative to conventional surfactants derived from fossil fuels.

Supplementary Materials: The following supporting information can be downloaded at https://www.mdpi.com/article/10.3390/fermentation10050257/s1, Figure S1. Fed-batch benchmark fermentation of *A. borkumensis* SK2 with bubble aeration and NH_4Cl as nitrogen source; Figure S2. Fed-batch benchmark fermentation of *A. borkumensis* SK2 with bubble-free membrane aeration and NH_4Cl as nitrogen source; Figure S3. DO-based fed-batch benchmark fermentation of *A. borkumensis* SK2 with bubble aeration and urea as nitrogen source; Figure S4. Ammonium and phosphate amount time course of the urea fed-batch fermentations; Figure S5. Combined antibacterial effect of chloramphenicol and tetracycline with glycine-glucolipid against different bacteria for MIC (<5% growth in terms of reached cell density) and IC50 (<50% growth) determination.

Author Contributions: Conceptualization, T.K., T.T. and S.K.; experimental work, T.K., M.K.L. and A.B.; methodology, T.K., S.K. and A.B.; validation, T.K. and S.K.; investigation, T.K., M.K.L., S.K. and A.B.; data curation, T.K., M.K.L. and A.B.; writing—original draft preparation, T.K. and S.K.; writing—review and editing, T.K., L.M.B., T.T., S.K., S.T. and K.-E.J.; visualization, T.K., M.K.L. and S.K.; supervision, T.T., L.M.B. and S.T.; project administration, T.T. and K.-E.J.; funding acquisition, T.T. and S.T. All authors have read and agreed to the published version of the manuscript.

Funding: T.K., L.M.B. and T.T. thank the German Federal Ministry of Education and Research (BMBF) for funding the project *GlycoX* (grant no. 161B0866B). S.K., S.T. and K.-E.J. thank the German Federal Ministry of Education and Research (BMBF) for funding the project *GlycoX* (grant no. 161B0866A). The laboratory of L.M.B. has been partially funded by the Deutsche Forschungsgemeinschaft (DFG, German Research Foundation) under Germany's Excellence Strategy—Exzellenzcluster 2186 The Fuel Science Center ID: 390919832.

Data Availability Statement: The raw data supporting the conclusions of this article will be made available by the authors on request.

Acknowledgments: We thank Patrick Bongartz and Moritz Meyer from BioThrust GmbH for supporting the bubble-free fermentation by providing us with the static membrane module. We also thank Isabel Schmidt for her experimental support.

Conflicts of Interest: The authors declare no conflicts of interest.

Abbreviations

μ_{max}	maximal growth rate in h^{-1}
C/N-ratio	carbon-to-nitrogen ratio in Cmol $Nmol^{-1}$
CTR	carbon dioxide transfer rate in mmol L^{-1} h^{-1}
DO	dissolved oxygen in %
F_{gas}	gas flow in L h^{-1}
N	stirring rate in min^{-1}
OTR	oxygen transfer rate in mmol L^{-1} h^{-1}
q_s	specific substrate uptake rate in g g^{-1} h^{-1}
RQ	respiratory quotient
r_s	volumetric substrate uptake rate in g L^{-1} h^{-1}
STY	space-time yield in mg L^{-1} h^{-1}
TMP	transmembrane pressure in bar
V_L	reactor filling volume in L
X_{O2}	oxygen proportion in the supply gas in %
$Y_{P/S}$	product-to-substrate yield in g g^{-1}
$Y_{P/X}$	product-to-biomass yield in g g^{-1}
$Y_{X/S}$	biomass-to-substrate yield in g g^{-1}

References

1. Abdel-Mawgoud, A.M.; Lépine, F.; Déziel, E. Rhamnolipids: Diversity of structures, microbial origins and roles. *Appl. Microbiol. Biotechnol.* **2010**, *86*, 1323–1336. [CrossRef] [PubMed]
2. Kubicki, S.; Bollinger, A.; Katzke, N.; Jaeger, K.-E.; Loeschcke, A.; Thies, S. Marine biosurfactants: Biosynthesis, structural diversity and biotechnological applications. *Mar. Drugs* **2019**, *17*, 408. [CrossRef] [PubMed]
3. Desai, J.D.; Banat, I.M. Microbial production of surfactants and their commercial potential. *Microbiol. Mol. Biol. Rev.* **1997**, *61*, 47–64. [CrossRef] [PubMed]
4. Schlebusch, I.; Pott, R.W.M.; Tadie, M. The ion flotation of copper, nickel, and cobalt using the biosurfactant surfactin. *Discov. Chem. Eng.* **2023**, *3*, 7. [CrossRef]
5. Van Delden, C.; Iglewski, B.H. Cell-to-cell signaling and *Pseudomonas aeruginosa* infections. *Emerg. Infect. Dis.* **1998**, *4*, 551–560. [CrossRef]
6. Tripathi, L.; Irorere, V.U.; Marchant, R.; Banat, I.M. Marine derived biosurfactants: A vast potential future resource. *Biotechnol. Lett.* **2018**, *40*, 1441–1457. [CrossRef] [PubMed]
7. Johann, S.; Seiler, T.-B.; Tiso, T.; Bluhm, K.; Blank, L.M.; Hollert, H. Mechanism-specific and whole-organism ecotoxicity of mono-rhamnolipids. *Sci. Total Environ.* **2016**, *548–549*, 155–163. [CrossRef] [PubMed]
8. Poremba, K.; Gunkel, W.; Lang, S.; Wagner, F. Toxicity testing of synthetic and biogenic surfactants on marine microorganisms. *Environ. Toxicol. Water Qual.* **1991**, *6*, 157–163. [CrossRef]
9. Santos, D.K.F.; Rufino, R.D.; Luna, J.M.; Santos, V.A.; Sarubbo, L.A. Biosurfactants: Multifunctional biomolecules of the 21st century. *Int. J. Mol. Sci.* **2016**, *17*, 401. [CrossRef]
10. Fischbach, M.A. Combination therapies for combating antimicrobial resistance. *Curr. Opin. Microbiol.* **2011**, *14*, 519–523. [CrossRef] [PubMed]
11. Patiño, A.D.; Montoya-Giraldo, M.; Quintero, M.; López-Parra, L.L.; Blandón, L.M.; Gómez-León, J. Dereplication of antimicrobial biosurfactants from marine bacteria using molecular networking. *Sci. Rep.* **2021**, *11*, 16286. [CrossRef] [PubMed]
12. Joshi-Navare, K.; Prabhune, A. A biosurfactant-sophorolipid acts in synergy with antibiotics to enhance their efficiency. *Biomed Res. Int.* **2013**, *2013*, 512495. [CrossRef] [PubMed]
13. Lydon, H.L.; Baccile, N.; Callaghan, B.; Marchant, R.; Mitchell, C.A.; Banat, I.M. Adjuvant antibiotic activity of acidic sophorolipids with potential for facilitating wound healing. *Antimicrob. Agents Chemother.* **2017**, *61*, e02547-16. [CrossRef] [PubMed]
14. Schneiker, S.; dos Santos, V.A.M.; Bartels, D.; Bekel, T.; Brecht, M.; Buhrmester, J.; Chernikova, T.N.; Denaro, R.; Ferrer, M.; Gertler, C.; et al. Genome sequence of the ubiquitous hydrocarbon-degrading marine bacterium *Alcanivorax borkumensis*. *Nat. Biotechnol.* **2006**, *24*, 997–1004. [CrossRef] [PubMed]
15. Yakimov, M.M.; Golyshin, P.N.; Lang, S.; Moore, E.R.B.; Abraham, W.; Lunsdorf, H.; Timmis, K.N. *Alcanivorax borkurmensis* gen. now, sp. nov., a new, hydrocarbon-degrading and surfactant-producing marine bacterium. *Int. J. Syst. Bacteriol.* **1998**, *48*, 339–348. [CrossRef] [PubMed]
16. Passeri, A.; Schmidt, M.; Haffner, T.; Wray, V.; Lang, S.; Wagner, F. Marine biosurfactants. IV. Production, characterization and biosynthesis of an anionic glucose lipid from the marine bacterial strain MM1. *Appl. Microbiol. Biotechnol.* **1992**, *37*, 281–286. [CrossRef]
17. Abraham, W.-R.; Meyer, H.; Yakimov, M. Novel glycine containing glucolipids from the alkane using bacterium *Alcanivorax borkumensis*. *Biochim. Biophys. Acta—Lipids Lipid Metab.* **1998**, *1393*, 57–62. [CrossRef]
18. Karmainski, T.; Dielentheis-Frenken, M.R.E.; Lipa, M.K.; Phan, A.N.T.; Blank, L.M.; Tiso, T. High-quality physiology of *Alcanivorax borkumensis* SK2 producing glycolipids enables efficient stirred-tank bioreactor cultivation. *Front. Bioeng. Biotechnol.* **2023**, *11*, 1325019. [CrossRef]
19. Kalscheuer, R.; Stöveken, T.; Malkus, U.; Reichelt, R.; Golyshin, P.N.; Sabirova, J.S.; Ferrer, M.; Timmis, K.N.; Steinbüchel, A. Analysis of storage lipid accumulation in *Alcanivorax borkumensis*: Evidence for alternative triacylglycerol biosynthesis routes in bacteria. *J. Bacteriol.* **2007**, *189*, 918–928. [CrossRef] [PubMed]
20. Manilla-Pérez, E.; Lange, A.B.; Luftmann, H.; Robenek, H.; Steinbüchel, A. Neutral lipid production in *Alcanivorax borkumensis* SK2 and other marine hydrocarbonoclastic bacteria. *Eur. J. Lipid Sci. Technol.* **2011**, *113*, 8–17. [CrossRef]
21. Sabirova, J.S.; Ferrer, M.; Lünsdorf, H.; Wray, V.; Kalscheuer, R.; Steinbüchel, A.; Timmis, K.N.; Golyshin, P.N. Mutation in a "tesB-Like" hydroxyacyl-coenzyme A-specific thioesterase gene causes hyperproduction of extracellular polyhydroxyalkanoates by *Alcanivorax borkumensis* SK2. *J. Bacteriol.* **2006**, *188*, 8452–8459. [CrossRef] [PubMed]
22. Manilla-Pérez, E.; Reers, C.; Baumgart, M.; Hetzler, S.; Reichelt, R.; Malkus, U.; Kalscheuer, R.; Wältermann, M.; Steinbüchel, A. Analysis of lipid export in hydrocarbonoclastic bacteria of the genus *Alcanivorax*: Identification of lipid export-negative mutants of *Alcanivorax borkumensis* SK2 and *Alcanivorax jadensis* T9. *J. Bacteriol.* **2010**, *192*, 643–656. [CrossRef] [PubMed]
23. Chang, Z.; Dai, W.; Mao, Y.; Cui, Z.; Zhang, Z.; Wang, Z.; Ma, H.; Chen, T. Enhanced 3-hydroxypropionic acid production from acetate via the Malonyl-CoA pathway in *Corynebacterium glutamicum*. *Front. Bioeng. Biotechnol.* **2022**, *9*, 808258. [CrossRef] [PubMed]
24. Lipphardt, A.; Karmainski, T.; Blank, L.M.; Hayen, H.; Tiso, T. Identification and quantification of biosurfactants produced by the marine bacterium *Alcanivorax borkumensis* by hyphenated techniques. *Anal. Bioanal. Chem.* **2023**, *415*, 7067–7084. [CrossRef] [PubMed]

25. Cui, J.; Hölzl, G.; Karmainski, T.; Tiso, T.; Kubicki, S.; Thies, S.; Blank, L.M.; Jaeger, K.-E.; Dörmann, P. The glycine-glucolipid of *Alcanivorax borkumensis* is resident to the bacterial cell wall. *Appl. Environ. Microbiol.* **2022**, *88*, e01126-22. [CrossRef] [PubMed]
26. Naether, D.J.; Slawtschew, S.; Stasik, S.; Engel, M.; Olzog, M.; Wick, L.Y.; Timmis, K.N.; Heipieper, H.J. Adaptation of the hydrocarbonoclastic bacterium *Alcanivorax borkumensis* SK2 to alkanes and toxic organic compounds: A physiological and transcriptomic approach. *Appl. Environ. Microbiol.* **2013**, *79*, 4282–4293. [CrossRef] [PubMed]
27. Abbasi, A.; Bothun, G.D.; Bose, A. Attachment of *Alcanivorax borkumensis* to hexadecane-in-artificial sea water emulsion droplets. *Langmuir* **2018**, *34*, 5352–5357. [CrossRef] [PubMed]
28. Godfrin, M.P.; Sihlabela, M.; Bose, A.; Tripathi, A. Behavior of marine bacteria in clean environment and oil spill conditions. *Langmuir* **2018**, *34*, 9047–9053. [CrossRef] [PubMed]
29. Rajpurohit, H.; Eiteman, M.A. Nutrient-limited operational strategies for the microbial production of biochemicals. *Microorganisms* **2022**, *10*, 2226. [CrossRef] [PubMed]
30. Saikia, R.R.; Deka, S.; Deka, M.; Banat, I.M. Isolation of biosurfactant-producing *Pseudomonas aeruginosa* RS29 from oil-contaminated soil and evaluation of different nitrogen sources in biosurfactant production. *Ann. Microbiol.* **2012**, *62*, 753–763. [CrossRef]
31. Moussa, T.A.A.; Mohamed, M.S.; Samak, N. Production and characterization of di-rhamnolipid produced by *Pseudomonas aeruginosa* TMN. *Braz. J. Chem. Eng.* **2014**, *31*, 867–880. [CrossRef]
32. Santos, A.S.; Sampaio, A.P.W.; Vasquez, G.S.; Anna, L.M.S.; Pereira, N.; Freire, D.M.G. Evaluation of different carbon and nitrogen sources in production of rhamnolipids by a strain of *Pseudomonas aeruginosa*. In *Biotechnology for Fuels and Chemicals*; Humana Press: Totowa, NJ, USA, 2002; Volume 223, pp. 1025–1035. [CrossRef]
33. Vennestrøm, P.N.R.; Osmundsen, C.M.; Christensen, C.H.; Taarning, E. Beyond petrochemicals: The renewable chemicals industry. *Angew. Chem. Int. Ed.* **2011**, *50*, 10502–10509. [CrossRef] [PubMed]
34. Wendisch, V.F.; Brito, L.F.; Gil Lopez, M.; Hennig, G.; Pfeifenschneider, J.; Sgobba, E.; Veldmann, K.H. The flexible feedstock concept in industrial biotechnology: Metabolic engineering of *Escherichia coli*, *Corynebacterium glutamicum*, *Pseudomonas*, *Bacillus* and yeast strains for access to alternative carbon sources. *J. Biotechnol.* **2016**, *234*, 139–157. [CrossRef] [PubMed]
35. Kiefer, D.; Merkel, M.; Lilge, L.; Henkel, M.; Hausmann, R. From acetate to bio-based products: Underexploited potential for industrial biotechnology. *Trends Biotechnol.* **2021**, *39*, 397–411. [CrossRef]
36. Lee, J.; Cha, S.; Kang, C.; Lee, G.; Lim, H.; Jung, G. Efficient conversion of acetate to 3-hydroxypropionic acid by engineered *Escherichia coli*. *Catalysts* **2018**, *8*, 525. [CrossRef]
37. Kim, Y.; Lama, S.; Agrawal, D.; Kumar, V.; Park, S. Acetate as a potential feedstock for the production of value-added chemicals: Metabolism and applications. *Biotechnol. Adv.* **2021**, *49*, 107736. [CrossRef] [PubMed]
38. Tremblay, P.-L.; Zhang, T. Electrifying microbes for the production of chemicals. *Front. Microbiol.* **2015**, *6*, 134494. [CrossRef] [PubMed]
39. Rabaey, K.; Rozendal, R.A. Microbial electrosynthesis—Revisiting the electrical route for microbial production. *Nat. Rev. Microbiol.* **2010**, *8*, 706–716. [CrossRef]
40. Cai, C.; Shi, Y.; Guo, J.; Tyson, G.W.; Hu, S.; Yuan, Z. Acetate production from anaerobic oxidation of methane via intracellular storage compounds. *Environ. Sci. Technol.* **2019**, *53*, 7371–7379. [CrossRef]
41. Kell, D.B. The transporter-mediated cellular uptake and efflux of pharmaceutical drugs and biotechnology products: How and why phospholipid bilayer transport is negligible in real biomembranes. *Molecules* **2021**, *26*, 5629. [CrossRef] [PubMed]
42. Kornberg, H. The role and control of the glyoxylate cycle in *Escherichia coli*. *Biochem. J.* **1966**, *99*, 1–11. [CrossRef] [PubMed]
43. Kiefer, D.; Merkel, M.; Lilge, L.; Hausmann, R.; Henkel, M. High cell density cultivation of *Corynebacterium glutamicum* on bio-based lignocellulosic acetate using pH-coupled online feeding control. *Bioresour. Technol.* **2021**, *340*, 125666. [CrossRef] [PubMed]
44. Merkel, M.; Kiefer, D.; Schmollack, M.; Blombach, B.; Lilge, L.; Henkel, M.; Hausmann, R. Acetate-based production of itaconic acid with *Corynebacterium glutamicum* using an integrated pH-coupled feeding control. *Bioresour. Technol.* **2022**, *351*, 126994. [CrossRef] [PubMed]
45. Axe, D.D.; Bailey, J.E. Transport of lactate and acetate through the energized cytoplasmic membrane of *Escherichia coli*. *Biotechnol. Bioeng.* **1995**, *47*, 8–19. [CrossRef] [PubMed]
46. Roe, A.J.; McLaggan, D.; Davidson, I.; O'Byrne, C.; Booth, I.R. Perturbation of anion balance during inhibition of growth of *Escherichia coli* by weak acids. *J. Bacteriol.* **1998**, *180*, 767–772. [CrossRef] [PubMed]
47. Leone, S.; Sannino, F.; Tutino, M.L.; Parrilli, E.; Picone, D. Acetate: Friend or foe? Efficient production of a sweet protein in *Escherichia coli* BL21 using acetate as a carbon source. *Microb. Cell Fact.* **2015**, *14*, 106. [CrossRef] [PubMed]
48. Xu, Q.; Bai, C.; Liu, Y.; Song, L.; Tian, L.; Yan, Y.; Zhou, J.; Zhou, X.; Zhang, Y.; Cai, M. Modulation of acetate utilization in *Komagataella phaffii* by metabolic engineering of tolerance and metabolism. *Biotechnol. Biofuels* **2019**, *12*, 61. [CrossRef] [PubMed]
49. Zhang, M.-M.; Zhao, X.-Q.; Cheng, C.; Bai, F.-W. Improved growth and ethanol fermentation of *Saccharomyces cerevisiae* in the presence of acetic acid by overexpression of SET5 and PPR1. *Biotechnol. J.* **2015**, *10*, 1903–1911. [CrossRef]
50. Lund, P.; Tramonti, A.; De Biase, D. Coping with low pH: Molecular strategies in neutralophilic bacteria. *FEMS Microbiol. Rev.* **2014**, *38*, 1091–1125. [CrossRef]

51. Schmollack, M.; Werner, F.; Huber, J.; Kiefer, D.; Merkel, M.; Hausmann, R.; Siebert, D.; Blombach, B. Metabolic engineering of *Corynebacterium glutamicum* for acetate-based itaconic acid production. *Biotechnol. Biofuels Bioprod.* **2022**, *15*, 139. [CrossRef] [PubMed]
52. Arnold, S.; Henkel, M.; Wanger, J.; Wittgens, A.; Rosenau, F.; Hausmann, R. Heterologous rhamnolipid biosynthesis by *P. putida* KT2440 on bio-oil derived small organic acids and fractions. *AMB Express* **2019**, *9*, 80. [CrossRef] [PubMed]
53. Palmqvist, E.; Hahn-Hägerdal, B. Fermentation of lignocellulosic hydrolysates. I: Inhibition and detoxification. *Bioresour. Technol.* **2000**, *74*, 17–24. [CrossRef]
54. Tiso, T.; Demling, P.; Karmainski, T.; Oraby, A.; Eiken, J.; Liu, L.; Bongartz, P.; Wessling, M.; Desmond, P.; Schmitz, S.; et al. Foam control in biotechnological processes—Challenges and opportunities. *Discov. Chem. Eng.* **2024**, *4*, 2. [CrossRef]
55. Vardar-Sukan, F. Foaming: Consequences, prevention and destruction. *Biotechnol. Adv.* **1998**, *16*, 913–948. [CrossRef]
56. Tiso, T.; Ihling, N.; Kubicki, S.; Biselli, A.; Schonhoff, A.; Bator, I.; Thies, S.; Karmainski, T.; Kruth, S.; Willenbrink, A.-L.; et al. Integration of genetic and process engineering for optimized rhamnolipid production using *Pseudomonas putida*. *Front. Bioeng. Biotechnol.* **2020**, *8*, 976. [CrossRef]
57. Junker, B. Foam and its mitigation in fermentation systems. *Biotechnol. Prog.* **2007**, *23*, 767–784. [CrossRef]
58. Delvigne, F.; Lecomte, J. Foam formation and control in bioreactors. In *Encyclopedia of Industrial Biotechnology*; Flickinger, M.C., Ed.; Wiley: Hoboken, NJ, USA, 2010. [CrossRef]
59. Routledge, S.J. Beyond de-foaming: The effects of antifoams on bioprocess productivity. *Comput. Struct. Biotechnol. J.* **2012**, *3*, e201210014. [CrossRef]
60. Anic, I.; Apolonia, I.; Franco, P.; Wichmann, R. Production of rhamnolipids by integrated foam adsorption in a bioreactor system. *AMB Express* **2018**, *8*, 122. [CrossRef] [PubMed]
61. Beuker, J.; Barth, T.; Steier, A.; Wittgens, A.; Rosenau, F.; Henkel, M.; Hausmann, R. High titer heterologous rhamnolipid production. *AMB Express* **2016**, *6*, 124. [CrossRef] [PubMed]
62. Bongartz, P.; Bator, I.; Baitalow, K.; Keller, R.; Tiso, T.; Blank, L.M.; Wessling, M. A scalable bubble-free membrane aerator for biosurfactant production. *Biotechnol. Bioeng.* **2021**, *118*, 3545–3558. [CrossRef] [PubMed]
63. Bongartz, P.; Karmainski, T.; Meyer, M.; Linkhorst, J.; Tiso, T.; Blank, L.M.; Wessling, M. A novel membrane stirrer system enables foam-free biosurfactant production. *Biotechnol. Bioeng.* **2023**, *120*, 1269–1287. [CrossRef]
64. Sha, R.; Meng, Q.; Jiang, L. The addition of ethanol as defoamer in fermentation of rhamnolipids. *J. Chem. Technol. Biotechnol.* **2012**, *87*, 368–373. [CrossRef]
65. Bator, I.; Karmainski, T.; Tiso, T.; Blank, L.M. Killing two birds with one stone—Strain engineering facilitates the development of a unique rhamnolipid production process. *Front. Bioeng. Biotechnol.* **2020**, *8*, 596414. [CrossRef] [PubMed]
66. Chen, C.-Y.; Baker, S.C.; Darton, R.C. Batch production of biosurfactant with foam fractionation. *J. Chem. Technol. Biotechnol.* **2006**, *81*, 1923–1931. [CrossRef]
67. Blesken, C.C.; Bator, I.; Eberlein, C.; Heipieper, H.J.; Tiso, T.; Blank, L.M. Genetic cell-surface modification for optimized foam fractionation. *Front. Bioeng. Biotechnol.* **2020**, *8*, 572892. [CrossRef] [PubMed]
68. Weiser, S.; Tiso, T.; Willing, K.; Bardl, B.; Eichhorn, L.; Blank, L.M.; Regestein, L. Foam-free production of the rhamnolipid precursor 3-(3-hydroxyalkanoyloxy) alkanoic acid (HAA) by *Pseudomonas putida*. *Discov. Chem. Eng.* **2022**, *2*, 8. [CrossRef]
69. Von Campenhausen, M.; Demling, P.; Bongartz, P.; Scheele, A.; Tiso, T.; Wessling, M.; Blank, L.M.; Jupke, A. Novel multiphase loop reactor with improved aeration prevents excessive foaming in rhamnolipid production by *Pseudomonas putida*. *Discov. Chem. Eng.* **2023**, *3*, 2. [CrossRef]
70. Takesono, S.; Onodera, M.; Ito, A.; Yoshida, M.; Yamagiwa, K.; Ohkawa, A. Mechanical control of foaming in stirred-tank reactors. *J. Chem. Technol. Biotechnol.* **2001**, *76*, 355–362. [CrossRef]
71. Willis, R.B.; Montgomery, M.E.; Allen, P.R. Improved method for manual, colorimetric determination of total Kjeldahl nitrogen using salicylate. *J. Agric. Food Chem.* **1996**, *44*, 1804–1807. [CrossRef]
72. Invally, K.; Ju, L. Increased rhamnolipid concentration and productivity achieved with advanced process design. *J. Surfactants Deterg.* **2020**, *23*, 1043–1053. [CrossRef]
73. Ramana, K.V.; Karanth, N.G. Factors affecting biosurfactant production using Pseudomonas aeruginosa CFTR-6 under submerged conditions. *J. Chem. Technol. Biotechnol.* **1989**, *45*, 249–257. [CrossRef]
74. Jahns, T. Regulation of urea uptake in *Pseudomonas aeruginosa*. *Antonie Van Leeuwenhoek* **1992**, *62*, 173–179. [CrossRef] [PubMed]
75. Solomon, C.; Collier, J.; Berg, G.; Glibert, P. Role of urea in microbial metabolism in aquatic systems: A biochemical and molecular review. *Aquat. Microb. Ecol.* **2010**, *59*, 67–88. [CrossRef]
76. Jahns, T.; Zobel, A.; Kleiner, D.; Kaltwasser, H. Evidence for carrier-mediated, energy-dependent uptake of urea in some bacteria. *Arch. Microbiol.* **1988**, *149*, 377–383. [CrossRef]
77. Silberbach, M.; Hüser, A.; Kalinowski, J.; Pühler, A.; Walter, B.; Krämer, R.; Burkovski, A. DNA microarray analysis of the nitrogen starvation response of *Corynebacterium glutamicum*. *J. Biotechnol.* **2005**, *119*, 357–367. [CrossRef] [PubMed]
78. Poremba, K.; Gunkel, W.; Lang, S.; Wagner, F. Marine biosurfactants, III. Toxicity testing with marine microorganisms and comparison with synthetic surfactants. *Z. Naturforschung C* **1991**, *46*, 210–216. [CrossRef] [PubMed]
79. Schulz, D.; Passeri, A.; Schmidt, M.; Lang, S.; Wagner, F.; Wray, V.; Gunkel, W. Marine biosurfactants, I. Screening for biosurfactants among crude oil degrading marine microorganisms from the North Sea. *Z. Naturforschung C* **1991**, *46*, 197–203. [CrossRef] [PubMed]

80. Bateman, A.; Martin, M.-J.; Orchard, S.; Magrane, M.; Ahmad, S.; Alpi, E.; Bowler-Barnett, E.H.; Britto, R.; Bye-A-Jee, H.; Cukura, A.; et al. UniProt: The Universal Protein Knowledgebase in 2023. *Nucleic Acids Res.* **2023**, *51*, D523–D531. [CrossRef] [PubMed]
81. Soberón-Chávez, G.; Lépine, F.; Déziel, E. Production of rhamnolipids by *Pseudomonas aeruginosa*. *Appl. Microbiol. Biotechnol.* **2005**, *68*, 718–725. [CrossRef] [PubMed]
82. Müller, M.M.; Hörmann, B.; Kugel, M.; Syldatk, C.; Hausmann, R. Evaluation of rhamnolipid production capacity of *Pseudomonas aeruginosa* PAO1 in comparison to the rhamnolipid over-producer strains DSM 7108 and DSM 2874. *Appl. Microbiol. Biotechnol.* **2011**, *89*, 585–592. [CrossRef]
83. Medina, G.; Juárez, K.; Díaz, R.; Soberón-Chávez, G. Transcriptional regulation of *Pseudomonas aeruginosa* rhlR, encoding a quorum-sensing regulatory protein. *Microbiology* **2003**, *149*, 3073–3081. [CrossRef] [PubMed]
84. Reis, R.S.; Pereira, A.G.; Neves, B.C.; Freire, D.M.G. Gene regulation of rhamnolipid production in *Pseudomonas aeruginosa*—A review. *Bioresour. Technol.* **2011**, *102*, 6377–6384. [CrossRef] [PubMed]
85. Roe, A.J.; O'Byrne, C.; McLaggan, D.; Booth, I.R. Inhibition of *Escherichia coli* growth by acetic acid: A problem with methionine biosynthesis and homocysteine toxicity. *Microbiology* **2002**, *148*, 2215–2222. [CrossRef]
86. Suzuki, T.; Yamane, T.; Shimizu, S. Mass production of poly-ß-hydroxybutyric acid by fed-batch culture with controlled carbon/nitrogen feeding. *Appl. Microbiol. Biotechnol.* **1986**, *24*, 370–374. [CrossRef]
87. Huschner, F.; Grousseau, E.; Brigham, C.J.; Plassmeier, J.; Popovic, M.; Rha, C.; Sinskey, A.J. Development of a feeding strategy for high cell and PHA density fed-batch fermentation of *Ralstonia eutropha* H16 from organic acids and their salts. *Process Biochem.* **2015**, *50*, 165–172. [CrossRef]
88. Garcia-Gonzalez, L.; De Wever, H. Acetic acid as an indirect sink of CO_2 for the synthesis of polyhydroxyalkanoates (PHA): Comparison with PHA production processes directly using CO_2 as feedstock. *Appl. Sci.* **2018**, *8*, 1416. [CrossRef]
89. Abd El-Salam, F.H. Synthesis, antimicrobial activity and micellization of gemini anionic surfactants in a pure state as well as mixed with a conventional nonionic surfactant. *J. Surfactants Deterg.* **2009**, *12*, 363–370. [CrossRef]
90. Falk, N.A. Surfactants as antimicrobials: A brief overview of microbial interfacial chemistry and surfactant antimicrobial activity. *J. Surfactants Deterg.* **2019**, *22*, 1119–1127. [CrossRef]
91. Sheikh, M.S.; Khanam, A.J.; Matto, R.H.; Kabir-ud-Din. Comparative study of the micellar and antimicrobial activity of gemini-conventional surfactants in pure and mixed micelles. *J. Surfactants Deterg.* **2013**, *16*, 503–508. [CrossRef]
92. Hisada, A.; Matsumoto, E.; Hirano, R.; Konomi, M.; Bou Khalil, J.Y.; Raoult, D.; Ominami, Y. Detection of antimicrobial impact on gram-negative bacterial cell envelope based on single-cell imaging by scanning electron microscopy. *Sci. Rep.* **2023**, *13*, 11258. [CrossRef]
93. Santi, I.; Manfredi, P.; Maffei, E.; Egli, A.; Jenal, U. Evolution of antibiotic tolerance shapes resistance development in chronic *Pseudomonas aeruginosa* infections. *mBio* **2021**, *12*, e03482-20. [CrossRef] [PubMed]
94. Liu, J.; Gefen, O.; Ronin, I.; Bar-Meir, M.; Balaban, N.Q. Effect of tolerance on the evolution of antibiotic resistance under drug combinations. *Science* **2020**, *367*, 200–204. [CrossRef] [PubMed]
95. Rossi, C.C.; Santos-Gandelman, J.F.; Barros, E.M.; Alvarez, V.M.; Laport, M.S.; Giambiagi-deMarval, M. *Staphylococcus haemolyticus* as a potential producer of biosurfactants with antimicrobial, anti-adhesive and synergistic properties. *Lett. Appl. Microbiol.* **2016**, *63*, 215–221. [CrossRef] [PubMed]
96. Ben Khedher, S.; Boukedi, H.; Dammak, M.; Kilani-Feki, O.; Sellami-Boudawara, T.; Abdelkefi-Mesrati, L.; Tounsi, S. Combinatorial effect of *Bacillus amyloliquefaciens* AG1 biosurfactant and *Bacillus thuringiensis* Vip3Aa16 toxin on *Spodoptera littoralis* larvae. *J. Invertebr. Pathol.* **2017**, *144*, 11–17. [CrossRef]
97. Park, J.O.; Liu, N.; Holinski, K.M.; Emerson, D.F.; Qiao, K.; Woolston, B.M.; Xu, J.; Lazar, Z.; Islam, M.A.; Vidoudez, C.; et al. Synergistic substrate cofeeding stimulates reductive metabolism. *Nat. Metab.* **2019**, *1*, 643–651. [CrossRef] [PubMed]